

Evaluation of Flaws in Ferritic Piping

ASME Code Appendix J: Deformation Plasticity Failure Assessment Diagram (DPFAD)

ASME Code Case N-494 describes an alternative procedure for evaluating flaws in LWR ferritic piping. The approach identified removes some unnecessary conservatism in existing procedures and facilitates more cost-effective evaluations. This report describes the methods and data used to develop the Code Case N-494 procedure.

INTEREST CATEGORIES

Nuclear seismic risk,
design, and qualification
Nuclear component
reliability
Nuclear plant life extension

KEYWORDS

Carbon steels
Fracture mechanics
BWR
PWR
Failure assessment
diagrams
Reactor piping

BACKGROUND Section XI of the ASME Boiler and Pressure Vessel Code and the Code of Federal Regulations require owners of nuclear power plants to periodically inspect pressure-boundary components to determine their structural integrity. Engineers use flaw acceptance standards of the ASME Code to determine whether components with flaws can return safely to service. Beginning in 1983, ductile fracture mechanics research results were used to develop improved and less conservative flaw evaluation procedures for the Section XI Code. Numerous methods, materials, flaw types, loading conditions, and component geometries make this an ongoing activity, with the improved procedures permitting more cost-effective inspection decisions. This project uses the deformation plasticity failure assessment diagram (DPFAD) to evaluate part-through axial and circumferential flaws in ferritic piping.

OBJECTIVE To provide supporting data and technical background for the evaluation procedures in the new ASME Code Case N-494.

APPROACH The principal investigator, in cooperation with the ASME Section XI Working Group on Flaw Evaluation, developed DPFAD into ASME Code format. The approach, which incorporates standard safety factors, was validated by comparison with experimental fracture data for axial and circumferential part-through-wall flaws in ferritic piping.

RESULTS The DPFAD procedure has been developed for ASME Code application to seamless or welded wrought ferritic piping, pipe fittings, and their associated weldments with axial and circumferential part-through-wall flaws. To apply the DPFAD procedure, the user needs to determine if assessment points fall within the relevant failure assessment diagram curve. If points are outside the diagram curve, the pipe must be repaired or replaced. The report summarizes DPFAD methods and the basis for Code Case N-494, including comparisons with experimental data.

EPRI PERSPECTIVE This report provides documentation of research conducted to support development of ASME Code Case N-494. The alternative procedure described in this code case was developed using the DPFAD approach to fracture mechanics and was verified by comparison with experimental data. In some flaw situations, this procedure will permit less conservative evaluations than the current

code. An example is when load ratios go beyond limits set by Appendix H. Overall, the DPFAD method complements other evaluation procedures in the code.

PROJECT

RP1757-34

Project Manager: Sam W. Tagart, Jr.

Nuclear Power Division

Contractor: Babcock & Wilcox Company

For further information on EPRI research programs, call
EPRI Technical Information Specialists (415) 855-2411.

Evaluation of Flaws in Ferritic Piping

ASME Code Appendix J: Deformation Plasticity Failure Assessment Diagram (DPFAD)

NP-7492
Research Project 1757-34

Final Report, August 1991

Prepared by
BABCOCK & WILCOX COMPANY
1563 Beeson Street
Alliance, Ohio 44601

Principal Investigator
J. M. Bloom

DISCLAIMER OF WARRANTIES AND LIMITATION OF LIABILITIES

THIS REPORT WAS PREPARED BY THE ORGANIZATION(S) NAMED BELOW AS AN ACCOUNT OF WORK SPONSORED OR COSPONSORED BY THE ELECTRIC POWER RESEARCH INSTITUTE, INC. (EPRI). NEITHER EPRI, ANY MEMBER OF EPRI, ANY COSPONSOR, THE ORGANIZATION(S) NAMED BELOW, NOR ANY PERSON ACTING ON BEHALF OF ANY OF THEM:

(A) MAKES ANY WARRANTY OR REPRESENTATION WHATSOEVER, EXPRESS OR IMPLIED, (I) WITH RESPECT TO THE USE OF ANY INFORMATION, APPARATUS, METHOD, PROCESS, OR SIMILAR ITEM DISCLOSED IN THIS REPORT, INCLUDING MERCHANTABILITY AND FITNESS FOR A PARTICULAR PURPOSE, OR (II) THAT SUCH USE DOES NOT INFRINGE ON OR INTERFERE WITH PRIVATELY OWNED RIGHTS, INCLUDING ANY PARTY'S INTELLECTUAL PROPERTY, OR (III) THAT THIS REPORT IS SUITABLE TO ANY PARTICULAR USER'S CIRCUMSTANCE; OR

(B) ASSUMES RESPONSIBILITY FOR ANY DAMAGES OR OTHER LIABILITY WHATSOEVER (INCLUDING ANY CONSEQUENTIAL DAMAGES, EVEN IF EPRI OR ANY EPRI REPRESENTATIVE HAS BEEN ADVISED OF THE POSSIBILITY OF SUCH DAMAGES) RESULTING FROM YOUR SELECTION OR USE OF THIS REPORT OR ANY INFORMATION, APPARATUS, METHOD, PROCESS, OR SIMILAR ITEM DISCLOSED IN THIS REPORT.

ORGANIZATION(S) THAT PREPARED THIS REPORT:

BABCOCK & WILCOX COMPANY



Printed on Recycled Paper

Prepared for
Electric Power Research Institute
3412 Hillview Avenue
Palo Alto, California 94304

EPRI Project Manager
S. W. Tagart, Jr.

Nuclear Component Reliability Program
Nuclear Power Division

Electric Power Research Institute and EPRI are registered service marks of Electric Power Research Institute, Inc.
Copyright © 1991 Electric Power Research Institute, Inc. All rights reserved.

ORDERING INFORMATION

Requests for copies of this report should be directed to Research Reports Center (RRC), Box 50490, Palo Alto, CA 94303, (415) 965-4081. There is no charge for reports requested by EPRI member utilities and affiliates, U.S. utility associations, U.S. government agencies (federal, state, and local), media, and foreign organizations with which EPRI has an information exchange agreement. On request, RRC will send a catalog of EPRI reports.

ABSTRACT

This report summarizes the methods and bases used by an ASME Code procedure for the evaluation of flaws in ferritic piping. The procedure is currently under consideration by the ASME Boiler and Pressure Vessel Code Committee of Section XI. The procedure was initially proposed in 1985 for the evaluation of the acceptability of flaws detected in piping during in-service inspection for certain materials, identified in Article IWB-3640 of the ASME Boiler and Pressure Vessel Code Section XI "Rules for In-service Inspection of Nuclear Power Plant Components," for which the fracture toughness is not sufficiently high to justify acceptance based solely on the plastic limit load evaluation methodology of Appendix C and IWB-3641. The procedure, referred to as Appendix J, originally included two approaches: a J-integral based tearing instability (J-T) analysis and the deformation plasticity failure assessment diagram (DPFAD) methodology. During the last few years, the DPFAD part of Appendix J was developed into Code format and with the support of the members of the ASME Section XI Working Group on Flaw Evaluation and the Electric Power Research Institute, Appendix J has been shown to be a valid approach for the assessment of both circumferential and axial part-through-the-wall flaws in ferritic piping.

In Appendix J, a general DPFAD approach was simplified for application to part-through wall flaws in ferritic piping through the use of a single DPFAD curve for circumferential flaws. Axial flaws are handled using two DPFAD curves where the ratio of flaw depth to wall thickness is used to determine the appropriate DPFAD curve. Flaws are evaluated in Appendix J by comparing the actual pipe applied stress with the allowable stress with the appropriate safety factors for the flaw size at the end of the evaluation period. Assessment points for circumferential and axial flaws are plotted on the appropriate failure assessment diagram. If the assessment points with the specified safety factors fall inside the appropriate failure assessment diagram curve, the inspection flaw is allowable. If the assessment points fall outside the diagram curve, the pipe must be repaired or replaced. In addition, this report summarizes the experimental test predictions of the results of the Battelle Columbus Laboratory experiments, the Eiber experiments, and the JAERI tests using the Appendix J DPFAD methodology. Lastly, this report also provides guidelines for handling residual stresses in the evaluation procedure.

ACKNOWLEDGEMENTS

The review and evaluation of the ASME Section XI Working Group on Flaw Evaluation and other interested individuals is acknowledged. In particular, R. C. Cipolla, J. P. Houstrop, S. Yukawa, E. Friedman, D. M. Norris, K. K. Yoon, and D. Scarth, are acknowledged for their contributions. Special thanks and recognition goes to D. Scarth who wrote Appendix B of this report and helped demonstrate the consistency of Appendix J-DPFAD to Appendix Z (Code Case N-463) in the limit load failure regime.

Part of the research reported here was sponsored by the Electric Power Research Institute under EPRI project RP 1757-34. Other portions of the development of Appendix J were sponsored by the Babcock & Wilcox company under Codes & Standards support. Additional thanks goes to D. M. Norris, former EPRI project manager, and to the current project manager, S. W. Tagart.

CONTENTS

<u>Section</u>	<u>Page</u>
1 INTRODUCTION	1 1
2 APPENDIX J PROCEDURE OVERVIEW	2 1
3 DETAILED FAILURE ASSESSMENT DIAGRAM ANALYSIS	3 1
FAILURE ASSESSMENT DIAGRAM CURVES	3-1
FAILURE ASSESSMENT DIAGRAM CUTOFFS	3-2
FAILURE ASSESSMENT POINT COORDINATES	3 4
FLAW ACCEPTANCE CRITERIA	3-7
CONSIDERATION OF RESIDUAL STRESSES	3 7
4 SIMPLIFICATION OF DPFAD FOR PART-THROUGH-THE-WALL FLAWS	4 1
GENERAL DPFAD APPROACH	4-1
GOALS OF SIMPLIFICATION OF DPFAD	4-3
MATERIAL CATEGORIES/STRESS-STRAIN PROPERTIES	4 3
GEOMETRY EFFECTS/CIRCUMFERENTIAL FLAWS	4-3
GEOMETRY EFFECTS/AXIAL FLAWS	4-4
LIMIT LOAD - s_f^{cutoff}	4 5
5 VALIDATION OF SIMPLIFIED APPROACH	5-1
CIRCUMFERENTIAL FLAWS	5-1
AXIAL FLAWS	5 2
6 CONCLUSIONS	6-1
7 REFERENCES	7-1
8 NOMENCLATURE	8-1
APPENDIX A - FAILURE ASSESSMENT CURVES	A-1
APPENDIX B - LIMIT LOAD - s_f^{cutoff}	B 1

ILLUSTRATIONS

<u>Figure</u>	<u>Page</u>
2-1 Failure Assessment Diagram Curve for Part-Through-the-Wall Circumferential Flaws.	2-3
2-2 Failure Assessment Diagram Curves for Part-Through-the-Wall Axial Flaws	2-4
3-1 Flaw Configurations for Circumferential and Axial Flaws	3-9
4-1 Illustration of Instability Point Determination	4-7
4-2 Comparison of Ferritic Material Categories for Axisymmetric Flaw for $a/t = 0.5$ and $R/t = 10$	4-8
4-3 Comparison of R/t Effects on DPFAD Curves for Through-Wall Circumferential Flaw Under Pure Bending	4-9
4-4 Comparison of Effects of Loading (Bending versus Tension) for Through-Wall Circumferential Flaw for 70XX SMAW Weld Metal	4-10
4-5 Comparison of θ Variation for Part-Through-the-Wall Flaw in Pipe When Tensile Loading for $a/t = 0.5$ for Ferritic Base Metal	4-11
4-6 Comparison of θ Variation for Part-Through-the-Wall Flaw in Pipe Under Tensile Loading for $a/t = 0.75$ for Ferritic Base Material	4-12
4-7 DPFAD Curve for Part-Through-the-Wall Flaw $\theta = 45$ degrees for Pipe Under Bending for $a/t = 0.5$ for Ferritic Base Metal	4-13
5-1 Failure Loading Locus per J_R Resistance Curve Plotted in DPFAD Space for BCL Pipe Test 4112-9	5-6
5-1 Failure Pressure Locus for J_R Resistance Curve Plotted in DPFAD Space for AEC 20 Pipe Test	5-7
5-3 Failure Pressure Locus per J_R Resistance Curve Plotted in DPFAD Space for AEC 8 Pipe Test	5-8

TABLES

<u>Table</u>	Page
2-1 Specified Safety Factor (SF)	2-2
4-1 Tensile Properties for DPFAD for Ferritic Piping Materials at 450-550°F	4-6
5-1 BCL Tests (CSC) Predictions Using Actual Material Properties	5-4
5-2 JAERI Pipe Tests (CSC)	5 5
5 3 EIBER/BCL Axial Flawed Pipe Burst Tests	5-5

Section 1

INTRODUCTION

Section XI of the ASME Code (1) and 10 CFR50 of the United States Code of Federal Regulations (2) require periodic inspection of reactor coolant pressure boundary components in operating commercial nuclear power plants. If flaws are found during inspection, evaluation using the acceptance standards of IWB-3500 in Section XI is required. Flaws larger than those specified in IWB-3500 can be evaluated further using the analysis procedures and acceptance criteria in IWB-3600.

Prior to 1983, evaluation procedures existed for only ferritic steel components four inches or greater in thickness. In the 1983 Winter Addenda to the ASME Code, procedures based on plastic collapse (limit load) for Class 1 austenitic steel piping were added. In 1985, revised evaluation procedures were incorporated in the Winter Addenda to the Code to allow consideration of certain low toughness welds where the possibility exists of failure mechanisms due to unstable flaw extension at loads lower than the plastic collapse loads. These revised computational procedures in the 1985 Addenda were based on elastic-plastic fracture mechanics methodology using conservative approximate correction factors applied to the limit load expressions. This evaluation methodology appeared in Appendix C and IWB-3641 of the 1985 Addenda.

In 1983, the Working Group on Flaw Evaluation of Section XI initiated work on the development of flaw evaluation procedures for ASME Class 1 ferritic piping. Flawed ferritic piping was recognized to have possible failure mechanisms which, depending on operating temperature, could range from linear elastic fracture to elastic plastic ductile tearing to plastic collapse. This wide variation of failure mechanisms necessitated an evaluation procedure which could account for all possible failure modes. The ASME Section XI Working Group on Flaw Evaluation approached this problem through the development of two separate appendices to the Code; Appendix Z (3) and Appendix J.

Appendix Z first appeared in the 1988 Winter Addenda as Code Case N-463 in answer to the inquiry: "Under Section XI, Division 1, may Class 1 ferritic piping containing a

flaw that exceeds the acceptance standards of IWB-3514.2 be evaluated and accepted for continued service as provided in IWB-3132.4?" Appendix Z consists of a simple, step by step screening criterion based on the deformation plasticity failure assessment diagram (DPFAD) approach (4) to identify the relevant failure mechanisms and appropriate analysis methods. Separate analysis procedures are provided for brittle fracture, ductile tearing, and plastic collapse. For ductile tearing, correction factors similar to those of Appendix C are used based on elastic-plastic J-integral solutions for through-wall flawed geometries using bounding stresses and lower bound material properties.

Appendix J developed in parallel with Appendix Z provides an alternate methodology using the DPFAD procedure (5) directly to determine acceptance of ferritic piping containing a flaw that exceeds the acceptance standards of IWB-3514.2. Flaws are evaluated in Appendix J by comparing the actual pipe applied stress with the allowable stress with the appropriate safety factors for the flaw size at the end of the evaluation period. Assessment points accounting for the actual pipe material properties through the input of the J_R resistance curve due to ductile flaw extension for circumferential and axial flaws are plotted on the appropriate failure assessment diagram. If the assessment points with the specified safety factors fall inside the appropriate failure assessment curve, the inspection flaw is allowable. If the assessment points fall outside the diagram curve, the pipe must be repaired or replaced. Appendix J addresses the current limitations of Appendix Z (Code Case N-463) by handling:

- all combinations of membrane and bending stress (Appendix Z is limited to piping systems with predominantly bending loads).
- residual stresses in the elastic-plastic failure regime (Appendix Z has no provision for handling residual stresses in the elastic-plastic failure mode).
- actual pipe material toughness properties through direct input into Appendix J of either the J_R resistance curve that characterizes ductile flaw extension, or the fracture toughness, J_{IC} (Appendix Z is limited to three levels of material toughness).
- the appropriate part-through wall flaw geometries based on published J-integral solutions (Appendix Z uses through-wall flawed geometries to generate approximate solutions for the part-through-the-wall geometries of interest).

This report will first address an overview of the Appendix J procedure followed by a detailed discussion of the procedure. Details of the simplification of the general DPFAD methodology for part-through wall flaws for ferritic piping used in Appendix J

will be presented and lastly, validation of the simplified approach through comparisons with actual experimental test results of degraded nuclear piping will be discussed.

Section 2

APPENDIX J PROCEDURE OVERVIEW

The following is a brief summary of the steps used to evaluate flaws in ferritic piping using the Appendix J procedure:

1. Determine the actual flaw configuration from the measured flaw in accordance with IWA-3000 of Section XI.
2. Resolve the actual flaw into circumferential and axial flaw components.
3. Determine the stresses normal to the flaw at the location of the detected flaw for normal operating (including upset and test) conditions and emergency and faulted conditions.
4. Perform a flaw growth analysis to establish the end of evaluation period flaw dimensions, a_f and l_f .
5. Obtain pipe material properties, E , σ_y , σ_u , and J_R or J_{IC} , at the temperatures required for analysis.
6. Select the appropriate failure assessment diagram curve from Figures 2-1 and 2-2 according to flaw configuration, circumferential or axial, and for axial flaws according to the ratio of flaw depth to wall thickness.
7. Calculate the vertical cutoff, S_F^{cutoff} , for the selected failure assessment diagram curve.
8. Calculate the assessment point coordinates (S'_F , K'_F) for the piping stresses P_m , P_b and P_e for circumferential flaws or p (pressure) for axial flaws using the specified safety factors in Table 2-1.
9. Plot the assessment point(s) calculated in step 8. on the appropriate failure assessment diagram and determine the acceptability of the pipe for continued service. The acceptability criteria is given in Section 3.

Table 2-1
Specified Safety Factors (SF)

	(SF)
Circumferential Flaws:	
Normal and Upset Conditions	2.77
Emergency and Faulted Conditions	1.39
Axial Flaws:	
Normal and Upset Conditions	3.0
Emergency and Faulted Conditions	1.5

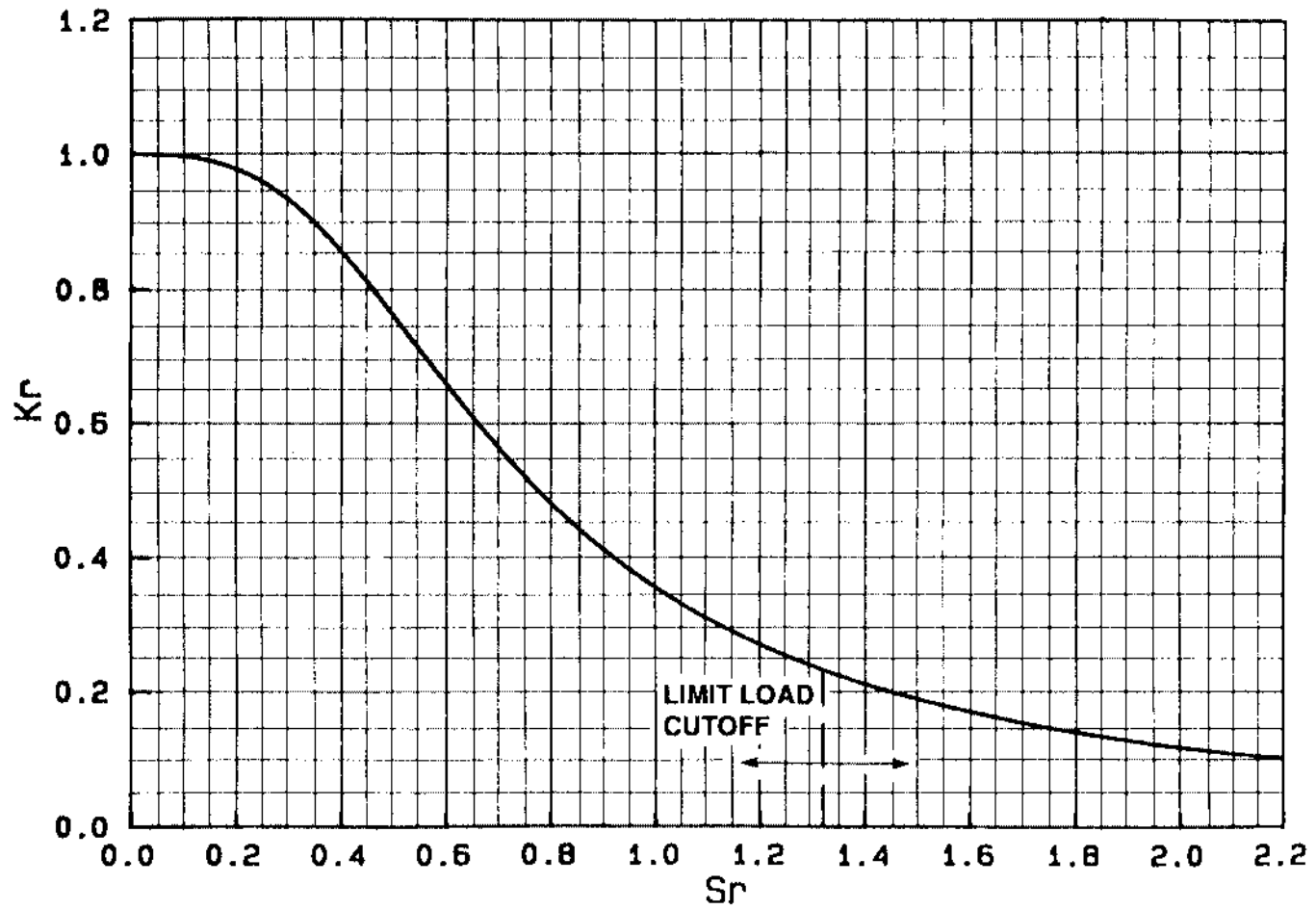


Figure 2-1 Failure Assessment Diagram Curve for Part-Through-the-Wall Circumferential Flaws.

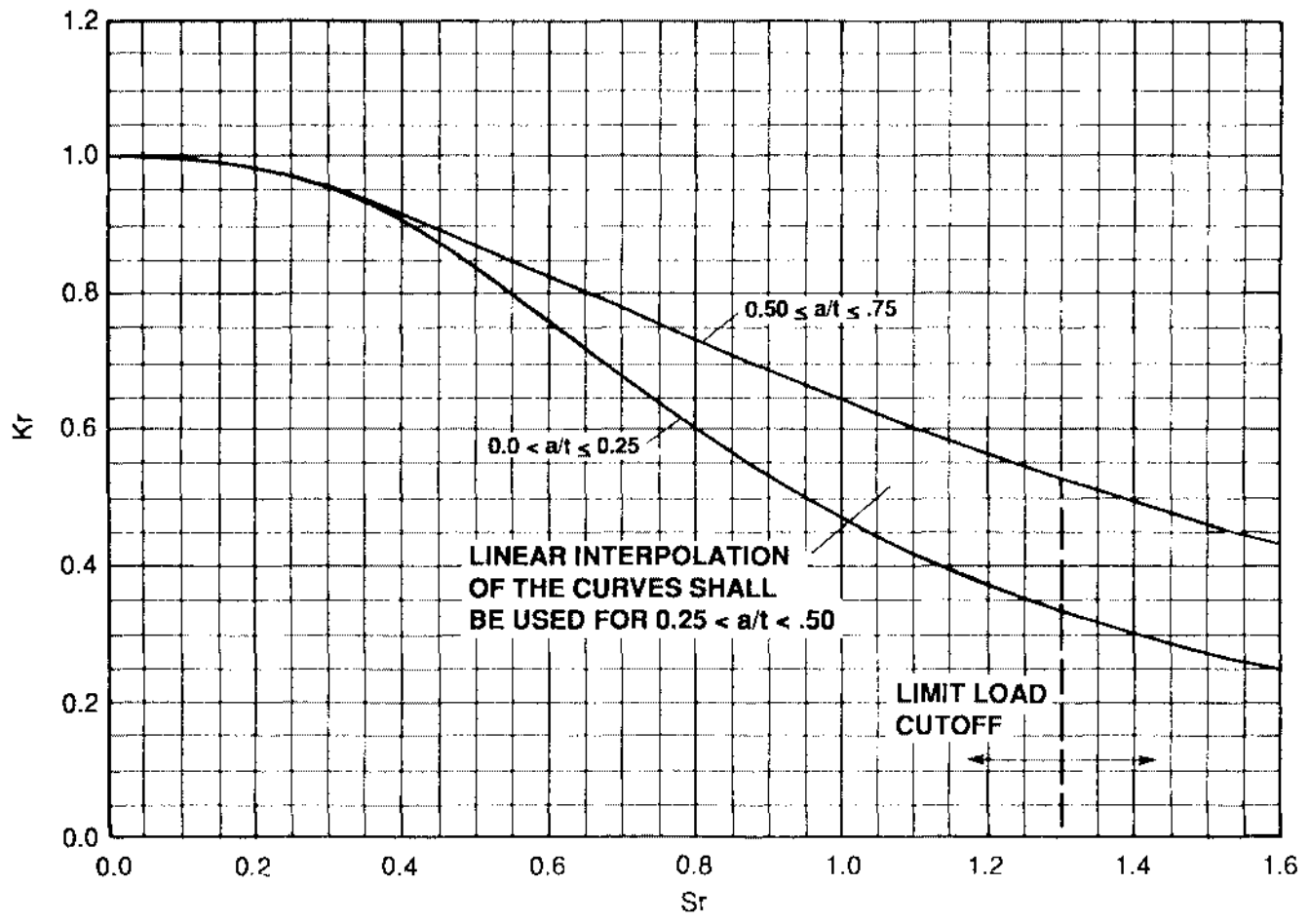


Figure 2-2 Failure Assessment Diagram Curves for Part-Through-the-Wall Axial Flaws

Section 3

DETAILED FAILURE ASSESSMENT DIAGRAM ANALYSIS

This section describes the detailed failure assessment diagram procedure for the evaluation of flaws in ferritic piping. The procedure involves:

- the choice of the failure assessment diagram curve.
- the calculation of the failure assessment point coordinates.
- the evaluation for flaw acceptance determination.

FAILURE ASSESSMENT DIAGRAM CURVES

Failure assessment diagram curves for ferritic piping are proposed for the following two flaw configurations:

- part through-the-wall circumferential flaws under any combination of primary membrane, primary bending, and expansion stresses.
- part through-the-wall axial flaws in pipes under internal pressure.

Figure 2-1 shall be used for part through-the-wall circumferential flaws of depths up to 75 percent of the pipe wall thickness and lengths up to one-half the inside circumference of the pipe.

Figure 2-2 shall be used for axial flaws of depths up to 75 percent of the pipe wall thickness and lengths up to l_{crit} , where l_{crit} is given by the limit load condition for through-the-wall flaws:

$$l_{crit} = 1.58 (Rt)^{1/2} [(\sigma_f/\sigma_h)^2 - 1]^{1/2} \quad (3-1)$$

In Figure 2-2, the ratio of flaw depth to wall thickness (a/t) shall be used to determine the appropriate failure assessment diagram curve. For the flaw depth

range from 25 percent to 50 percent of the wall thickness ($0.25 < a/t < 0.50$) linear interpolation of the failure assessment diagram curves shall be used. Linear interpolation is to be made based on a straight line drawn from the origin of the failure assessment diagram.

FAILURE ASSESSMENT DIAGRAM CUTOFFS

The failure assessment diagram curves shown in Figures 2-1 and 2-2 shall have vertical cutoffs for upper bound limits on S_r . These cutoffs are discussed as follows with additional details given in Appendix B.

For the circumferential flaw cutoff for pure membrane stress ($P_b=0$) the limit load cutoff for S_r is given by:

$$S_r^{\text{cutoff}} = P_{m1}/P'_m \quad (3-2)$$

where

$$P_{m1} = \sigma_f [1 \cdot (a/t)(\theta/\pi) - 2\psi/\pi] \quad (3-3)$$

$$\psi = \text{Arc sin } (0.5 (a/t) \sin \theta) \quad (3-4)$$

$$P'_m = \sigma_y \gamma \Gamma_m \quad (3-5)$$

where Γ is defined below.

For membrane plus bending stresses, the limit load cutoff for S_r is given by:

$$S_r^{\text{cutoff}} = P_b/P'_m \quad (3-6)$$

where

$$P'_m = \sigma_y \gamma \Gamma_m (P_b/P_m) \text{ for } P_m \neq 0 \quad (3-7)$$

$$P'_m = (4/\pi) \sigma_y \Gamma_m \text{ for } P_m=0 \quad (3-8)$$

$$\gamma = \frac{-\pi}{8} \frac{P_b}{P_m} + \left[\left(\frac{\pi P_b}{8 P_m} \right)^2 + 1 \right]^{0.5} \quad (3-9)$$

$$r_m = \frac{[R_2^2 - R_C^2 + (1 - \frac{\theta}{\pi}) (R_C^2 - R_1^2)]}{[R_2^2 - R_1^2]} \quad (3-10)$$

$$R_C = R_1 + a \quad (3-11)$$

For circumferential flaws not penetrating the compressive region of the pipe cross-section ($\theta + \beta \leq \pi$) (see Figure 3-1)

$$P_b' = \frac{2\sigma_f}{\pi} [2 \sin\beta - (a/t) \sin \theta] \quad (3-12)$$

where

$$\beta = \frac{1}{2} \left[\pi - \frac{a}{t} \theta - \frac{\pi(SF)P_m}{\sigma_f} \right] \quad (3-13)$$

For longer flaws penetrating the compressive region of the pipe cross-section ($\theta + \beta > \pi$),

$$P_b' = \frac{2\sigma_f}{\pi} \left(2 - \frac{a}{t} \right) \sin \beta \quad (3-14)$$

where

$$\beta = \frac{\pi}{2 - a/t} \left[1 - a/t - \frac{(SF)P_m}{\sigma_f} \right] \quad (3-15)$$

The safety factor (SF) is given in Table 2-1.

For axial flaws in pipes under internal pressure the limit load cutoff for S_r is given by:

$$S_r^{\text{cutoff}} = \frac{\sigma_1 t}{R_1 P_0} \quad (3-16)$$

where

$$P_0 = \frac{2}{\sqrt{3}} \frac{(t - a^*)}{(R_1 + a^*)} \sigma_y \quad (3-17)$$

and

$$a^* = \frac{a[1-(1+1^2/2t^2)^{-1/2}]}{[1-a/t(1+1^2/2t^2)^{-1/2}]} \quad (3-18)$$

and

$$\sigma = \sigma_f [(1-x)/(1-x/M_2)] \quad (3-19)$$

where

$$x = a/t$$

$$M_2 = [1 + (1.61/(4 Rt))^2]^{0.5} \quad (3-20)$$

FAILURE ASSESSMENT POINT COORDINATES

Failure assessment point coordinates denoted by (S'_f, K'_f) shall be calculated for the end of the evaluation period flaw dimensions and for stresses at the location of, and normal to, the flaw using the J_R resistance curve data for elastic-plastic fracture where ductile flaw extension at upper shelf temperatures may occur prior to reaching limit load, or J_{IC} fracture toughness data at transition or lower shelf temperatures.

The equations necessary to calculate the failure assessment point coordinates (S'_f, K'_f) for part through-the-wall circumferential flaws for ductile flaw extension, Δa , are given below. The relevant crack dimensions for the computations are shown in Figure 3-1. When the temperature is in the transition or lower shelf region, J_R should be replaced by J_{IC} and Δa set to zero.

$$S'_f = (SF)P'_m/P'_m \quad (3-21)$$

where SF is given in Table 2-1 and P'_m is re-calculated for each value of Δa . If the primary membrane stress P_m is not zero,

$$P'_m = \sigma_y \gamma \Gamma_m \quad (3-22)$$

$$\gamma = -\frac{\pi}{8} \frac{P_b}{P_m} + \left[\left(\frac{\pi}{8} \frac{P_b}{P_m} \right)^2 + 1 \right]^{0.5} \quad (3-23)$$

$$\Gamma_m = \frac{[R_2^2 - R_c^2 + (1 - \frac{\theta}{\pi}) (R_c^2 - R_1^2)]}{[R_2^2 - R_1^2]} \quad (3-24)$$

$$R_c = R_1 + a + \Delta a \quad (3-25)$$

where Γ_m is re-calculated for each value of Δa .

When the primary membrane stress P_m is zero, then

$$S'_I = \frac{\pi P_b (SF)}{4 \sigma_y \Gamma_m} \quad (3-26)$$

where Γ_m is re-calculated for each value of Δa .

The coordinate K'_I is given by

$$K'_I = \sqrt{J_e/J_R(\Delta a)} \quad \text{for any value of } P_m \quad (3-27)$$

where J_e and J_R are also re-calculated for each value of Δa .

The elastic J-integral is given by

$$J_e = 1000 K_I^2/E' \quad (3-28)$$

where

$$K_I = (SF) P_m \sqrt{\pi a'} F_m \quad (3-29)$$

$$+ \{(SF) P_b + P_e\} \sqrt{\pi a'} F_b$$

$$F_m = 1.1 + (a'/t) \left[0.15241 + 16.722 \left(\frac{a'}{t} \frac{\theta}{\pi} \right)^{0.855} - 14.944 \left(\frac{a'}{t} \frac{\theta}{\pi} \right) \right] \quad (3-30)$$

$$F_b = 1.1 + (a'/t) \left[-0.09967 + 5.0057 \left(\frac{a'}{t} \frac{\theta}{\pi} \right)^{0.565} - 2.8329 \left(\frac{a'}{t} \frac{\theta}{\pi} \right) \right] \quad (3-31)$$

$$a' = a + \Delta a \quad (3-32)$$

In the above equations, a' is updated after each increment of ductile flaw extension, while θ is fixed at its end of evaluation period value.

The equations necessary to calculate the failure assessment point coordinates (S_f' , K_f') for axial flaws for ductile flaw extension, Δa , are given below. When the temperature is in the transition or lower shelf region, J_R should be replaced by J_{IC} and Δa set to zero.

$$S_f' = (SF)p/P_0 \quad (3-33)$$

where SF is given in Table 2-1 and P_0 is re-calculated for each value of Δa from,

$$P_0 = \frac{2}{\sqrt{3}} \frac{(t-a^*)}{(R_1 + a^*)} \sigma_y \quad (3-34)$$

$$a^* = \frac{a' \{1 - [1 + 0.5 (a'/t)^2 / (a/l)^2]^{-1/2}\}}{[1 - (a'/t) [1 + 0.5 (a'/t)^2 / (a/l)^2]^{-1/2}} \quad (3-35)$$

The coordinate K_f' is given by Eq. 3-27

where

$$K_I = (SF) p (R_1/t) \sqrt{\pi a'/Q} F_1 \quad (3-36)$$

$$Q = 1 + 4.593 (a/l)^{1.65} \quad (3-37)$$

$$F_1 = 0.97 [M_1 + M_2 (a'/t)^2 + M_3 (a'/t)^4] f_c \quad (3-38)$$

$$f_c = [(R_2^2 + R_1^2)/(R_2^2 - R_1^2) + 1 - 0.5\sqrt{a'/t}] t/R_1 \quad (3-39)$$

$$M_1 = 1.13 - 0.18 (a/l) \quad (3-40)$$

$$M_2 = -0.54 + 0.445/(0.1+a/l) \quad (3-41)$$

$$M_3 = 0.5 - \frac{1}{(0.65+2a/l)} + 14 (1-2a/l)^{24} \quad (3-42)$$

In the equations above, a' is updated after each increment of ductile flaw extension, while a/l is fixed at its end of evaluation period value.

FLAW ACCEPTANCE CRITERIA

The failure assessment point coordinates (S'_f , K'_f) are calculated for each loading condition using the safety factors (SF) given in Table 2-1 to determine flaw acceptance.

- (a) For lower shelf and transition temperatures, Δa is set to zero and J_R is set to the J_{IC} at the temperature of interest in the calculation of the failure assessment point coordinate. Plot the assessment point on the appropriate failure assessment diagram. The assessment point must be inside the failure assessment curve in order to have the flawed pipe accepted for continued service.
- (b) For upper shelf temperatures where ductile flaw extension may occur prior to reaching limit load, a series of assessment points for various amounts of ductile flaw extension, Δa , obtained from the J_R resistance curve shall be calculated and plotted on the appropriate failure assessment diagram. One or more of the calculated assessment points must be inside the failure assessment curve in order to have the flawed pipe accepted for continued service.
- (c) In addition to satisfying (a) and (b), the S'_f coordinate of the assessment point must also satisfy

$$S'_f \leq S_f^{\text{cutoff}} \quad (3-43)$$

where S_f^{cutoff} is the limit load cutoff on the failure assessment diagram.

CONSIDERATION OF RESIDUAL STRESSES

Appendix J unlike Appendix Z can account for the effects of residual stresses not only in the linear elastic regime but in the elastic-plastic regime as well. The more exact DPFAD methodology for accounting for residual stresses documented in (6) has been simplified for Appendix J. The procedure is given as follows for Appendix J. If the residual stress distribution is known, calculate the stress intensity factor due to this residual stress distribution for the flaw size of interest and denote it by $K_{II}^R(a)$. If $K_{II}^R(a) \leq 0$, ignore the effects of residual stresses in the assessment. If $K_{II}^R(a) > 0$, calculate ρ , a term which approximately corrects for the elastic-plastic effects of the self equilibrating secondary (residual stress loading) stresses. Expressions for calculating ρ documented in (22) are as follows:

$$\rho = (1-Z) \quad \text{for } Z \leq 0.58 \quad (3-44)$$

$$\rho = 0.8 (1-Z)^{0.74} \quad \text{for } Z > 0.58 \quad (3-45)$$

where

$$Z = \text{SQRT} [(a+\Delta a)/(a+\Delta a+R_y)] \quad (3-46)$$

and

$$R_y = (K_I^S(a+\Delta a)/\sigma_y)^2/(2\pi) \quad (3-47)$$

R_y is the radius of the plastic zone for plane stress conditions, σ_y is the yield strength of the material.

Next calculate K_I^{TOTAL} as follows:

$$K_I^{\text{TOTAL}} = K_I^I(a+\Delta a) + K_I^S(a+\Delta a) + \rho(a+\Delta a) \quad (3-48)$$

where

$K_I^I(a+\Delta a)$ is given by Eq. 3-37 and

$$K_I^S(a+\Delta a) = [1000 [K_I^S(a+\Delta a)]^{2/E'J_R(\Delta a)}]^{0.5} \quad (3-49)$$

Once K_I^{TOTAL} is calculated from Eq. 3-48, the assessment points are plotted on the DPFAD figure which is appropriate to the flaw orientation (circumferential or axial). The S_I^{TOTAL} coordinate is calculated per Eq. 3-21 or Eq. 3-33. The determination of flaw acceptance is the same as without the residual stresses,

namely, the new assessment point(s) (K_I^{TOTAL} , S_I^{TOTAL}) is (are) plotted on the appropriate failure assessment diagram. If the point or points fall inside the failure assessment curve, then the flawed pipe is acceptable for continued service.

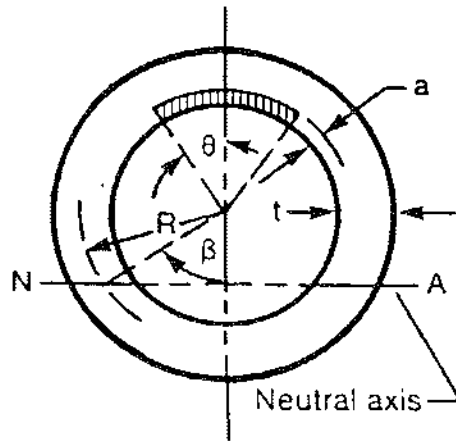


Figure 3-2a. Circumferential Flaw

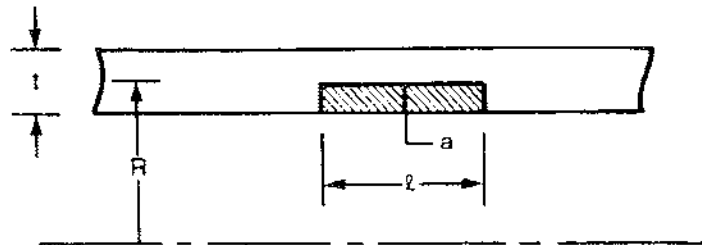


Figure 3-2b. Axial Flaw

Figure 3-1 Flaw Configurations for Circumferential and Axial Flaws

Section 4

SIMPLIFICATION OF DPFAD FOR PART THROUGH-THE WALL FLAWS

The deformation plasticity failure assessment diagram (DPFAD) procedure utilizes deformation plasticity solutions (7,8) for cracked structures in the format of the British Central Electricity Generating Board's (CEGB) R-6 two criteria failure assessment diagram (FAD) (9) to graphically solve elastic plastic fracture mechanics problems through the solution of the nonlinear equation $J_{\text{applied}} = J_{\text{material}}$ for the load corresponding to the current crack length and tearing resistance. Since DPFAD was developed from the original CEGB two-criteria (10) approach, it not only handles elastic plastic fracture but linear elastic fracture and net section plastic collapse or limit load of the flawed structure. DPFAD, however, is more accurate than the R-6 procedure since DPFAD accounts for the actual material tensile properties through the Ramberg-Osgood representation, as well as the geometry of the flawed structure.

GENERAL DPFAD APPROACH

The general DPFAD procedure involves three steps:

The generation of the DPFAD curve from elastic plastic analysis of a flawed structure using deformation plasticity solutions for a simple power-law strain-hardening material based on the Ramberg-Osgood stress-strain equation:

$$\epsilon/\epsilon_0 = \sigma/\sigma_0 + \alpha(\sigma/\sigma_0)^n \quad (4-1)$$

where

$$\sigma_0 = \sigma_y \text{ and } \epsilon_0 = \sigma_y/E$$

If the J-integral response of the structure can be represented by

$$J_{\text{applied}} = J_{\text{I}}^e + J_{\text{p}} \quad (4-2)$$

then

$$\frac{J_{\text{applied}}}{G} = \frac{1}{K_I^2} \cdot (J_I^e + J_p)/G \quad (4-3)$$

or

$$K_I = \sqrt{G/J_{\text{applied}}} \cdot f(S_r) \quad (4-4)$$

where S_r is the ratio of applied stress to net section plastic collapse stress and

$$G = K_I^2 / K' \quad (4-5)$$

The difference between J_I^e and G is that J_I^e includes the small scale, yielding plastic zone correction while G does not. The resulting expression (4-4) defines a curve in the K_I - S_r plane which is a function of flaw geometry, structural configuration and stress-strain behavior of the material defined uniquely by α , n from Eq. 4-1. Because both K_I , S_r are linear in applied stress, the DPFAD curve is independent of the magnitude of applied loading.

The determination of assessment points based on the ratio of K_I or J_I (square root) of the structure divided by the relevant material property K_{IC} or J_{IC} (square root) at flaw initiation or for stable flaw growth, $J_R(\Delta a)$, (square root), the tearing resistance of the material for the ordinate, K_I' , and the ratio of the applied stress (load) to net section plastic collapse (limit load) for the abscissa, S_r' . For flaw initiation, a single assessment point is calculated. For stable crack growth, a locus of assessment points are determined by incrementing the crack size "a" by "a+ Δa " in the calculation of J_I for a constant applied load. The resulting locus is illustrated in Figure 4-1 in the shape of a "candy-cane".

Crack initiation or tearing instability can be determined graphically by plotting the calculated assessment point(s) on the failure assessment diagram. For crack initiation, the single assessment point must fall on the DPFAD curve or outside the curve. For tearing instability, the critical instability load is determined by the tangency of the assessment locus with the DPFAD curve as shown in Figure 4-1. Any assessment point on a line from the origin of the diagram is directly proportional to load with any other point on that same line and only one load level is needed to determine the instability load. The instability load is obtained by multiplying the applied load by the ratio of the distance from the origin to the point of intersection of the line with the DPFAD curve to the distance from the origin of the diagram to the applied load point.

GOALS OF SIMPLIFICATION OF DPFAD

The goal for simplification of the DPFAD methodology for part-through-the-wall flaws in ferritic piping is to be able to handle all materials, flaw sizes, and pipe sizes with a minimum of DPFAD curves. The determination of the assessment points requires only the stress intensity factor and limit load expressions for the various flaw configurations, loading states, and pipe sizes. Formulations for J_I for circumferential through-the-wall and part-through-the-wall flaws in cylinders under tension, bending, and combined bending and tension from (11) were used to generate DPFAD curves using PCFAD (12) for various combinations of α, n .

MATERIAL CATEGORIES/STRESS-STRAIN PROPERTIES

The initial comparisons of DPFAD curves were thought to require separate curves for each category of materials. Table 4-1 lists the tensile properties for ferritic piping materials required in order to compare the various DPFAD curves per α, n . The values of yield and ultimate strength were obtained from a study in (13). The values of α, n were determined using equations from (13) knowing only σ_y , σ_u , and E . Figure 4-2 shows a comparison of DPFAD curves for the four categories of materials given in Table 4-1 for an axisymmetric crack under tension for a flaw depth of 50% of the wall thickness for a radius to thickness ratio of 10. From this figure it can be concluded that ferritic piping could be categorized according to only three groups of materials:

- base metal and 70XX SMAW welds
- SAW welds
- 80XX SMAW welds

However, work in (15) has shown that a flawed pipe with a weld can be evaluated using the stress-strain properties of the base metal and the toughness properties of the weldment. Therefore, the DPFAD curve for ferritic piping can be represented by curves for the various flawed geometries of the pipe and the stress-strain properties of the base metal.

GEOMETRY EFFECTS/CIRCUMFERENTIAL FLAWS

For a particular material, the effects of pipe geometry, loading, and crack depth to wall thickness (a/t) were investigated. Figure 4-3 illustrates the effects of

radius to thickness (R/t) and it can be seen that this parameter has little effect on the DPFAD curves. Figure 4-4 illustrates the effect of tension versus bending for a through-the-wall flaw in a cylinder with $R/t = 10$. Again it can be seen that the pipe loading has little effect on the DPFAD curves. Once part-through-the-wall flaw J solutions were available (11), the effect of crack angle was investigated for $a/t = 0.5, 0.75$ for both bending and axial loadings. Figure 4-5 illustrates the effect of crack angle for $a/t = 0.5$ for axial loading. Figure 4-6 illustrates the same but for $a/t = 0.75$ and Figure 4-7 illustrates the effect of bending versus axial loading through comparison with the lower bound curve of Figure 4-6. Note that in both Figures 4-5 and 4-6 that the $2\theta = 27.5^\circ, 45^\circ, 90^\circ$ and 180° DPFAD curves all fall close to one another with the $2\theta = 90^\circ$ forming a lower bound. Figure 4-7 along with Figure 4-5 shows (as also demonstrated earlier in Figure 4-4) that the DPFAD curves are independent of the loading condition with the axial loading curve being slightly lower. Therefore, for part-through-the-wall circumferential flaws in ferritic piping, one DPFAD curve with lower bound stress-strain curve base metal properties for a geometry of $a/t = 0.5, R/t = 10$ and $2\theta = 90^\circ$ under axial loading can be used to represent all flawed ferritic pipes provided the correct stress intensity factor and limit load expressions are used in the calculation of the assessment points, K_I^L, S_I^L along with the appropriate toughness for the flawed region (weld or base metal) in terms of J_{IC} or $J_R(\Delta a)$. The resultant DPFAD curve for part-through-the-wall circumferential flaws in a ferritic pipe for $2\theta \leq 180^\circ$ is shown in Figure 2-1. Appendix A gives the equations for this curve as well as the coordinate points.

GEOMETRY EFFECTS/AXIAL FLAWS

For part-through-the-wall axial flaws in ferritic piping under pressure loading, similar comparisons have been made to illustrate the effects of flaw depth to wall thickness and aspect ratio (flaw depth to flaw length). While aspect ratio and pipe size have been shown to be insignificant (16),(17), flaw depth to wall thickness for axial flaws must be accounted for in the DPFAD curves. Two DPFAD curves shown in Figure 2-1 for lower bound ferritic base metal for part-through-the-wall axial flaws in pipes under pressure loading are needed in the assessment of defects using the DPFAD approach. The two curves in Figure 2-1 were developed from solutions for a continuous axial flaw in a cylinder with $R/t = 10$ for a flaw depth-to-wall thickness ratio of $a/t = 0.125$ for the lower curve and $a/t = 0.625$ for the upper curve for lower bound ferritic base metal. The DPFAD for axial part-through-the-wall flaw for $a/t = 0.25$ and $a/l = 0.167$ falls on this lower curve while the $a/t = 0.50, a/l = 0.167$ curve falls slightly higher than the continuous flaw DPFAD curve for $a/t = 0.625$. Limited evaluations comparing the various DPFAD curves seem to show that the

DPFAD curves saturate to the $a/t = 0.125$ lower bound curve for the continuous axial flaw. For axial flaws, the DPFAD curves also appear to be independent of the location of the flaw (inside versus outside) as demonstrated in (17). Appendix A gives the equations for these axial DPFAD curves as well as the coordinate points.

LIMIT LOAD - S_f^{cutoff}

The vertical cutoff of the DPFAD curves were originally set by

$$S_f^{\text{cutoff}} = \sigma_u / \sigma_y \quad (4-6)$$

This was demonstrated in (14) where a modified Ramberg-Osgood curve accounting for ultimate or saturation stress was used to generate a DPFAD curve for an infinite center-cracked plate. Since S_f^{cutoff} is defined in this report using the yield strength of the material, the actual material in the DPFAD plane would saturate out at approximately

$$S_r^{\text{cutoff}} = P/P_{\text{ultimate}} \times \sigma_u / \sigma_y = \frac{\sigma_u}{\sigma_y} \quad (4-7)$$

However, to make this cutoff consistent with the limit load expressions given in Appendix Z (3) of Code Case N-463, limit load failure is assumed to occur at a critical flow stress, σ_f , which is defined as the average of σ_y and σ_u . Using this as well as the limit load expressions in Appendix Z (3) will modify the vertical cutoffs in the general DPFAD approach resulting in Eqs. 3-2 and 3-16 for the circumferential and axial flaw, respectively. Further discussions can be found in Appendix B.

Table 4-1

Tensile Properties For DPFAD
For Ferritic Piping Materials
at 450 550°F

<u>MATERIAL</u>	<u>CONDITION</u>	<u>YS (ksi)</u>	<u>UTS (ksi)</u>	<u>m*</u>	<u>n*</u>	<u>DPFAD CUTOFF</u>
Base Metal	-----	31	65	2.64	4.42	2.10
70XX SMAW	PWHT	34	61	2.48	5.25	1.79
80XX SMAW	PWHT	73	88	1.62	10.78	1.21
SAW	PWHT	50	72	1.98	7.14	1.44

E = 26 x 10³ (ksi)

*Bloom's equation (EPRI NP-2431)

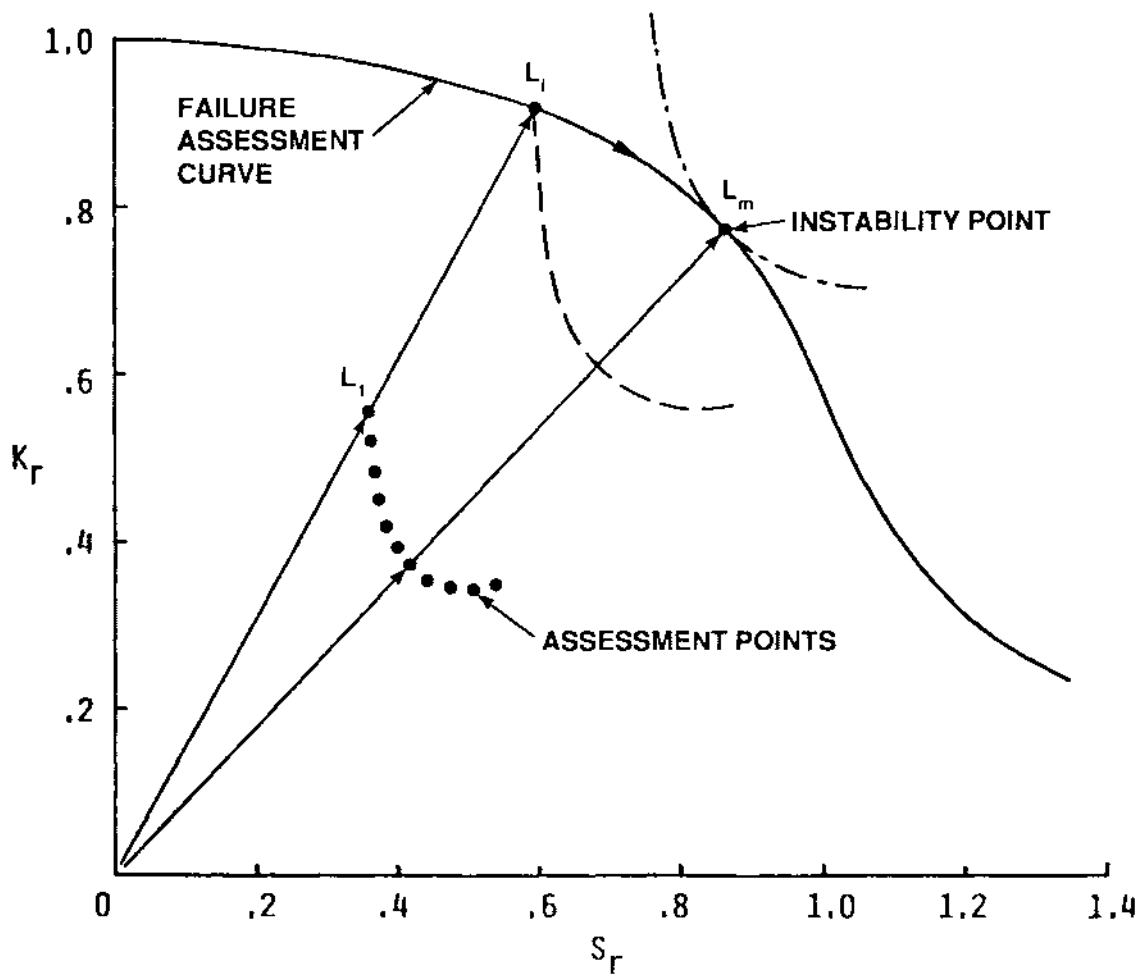


Figure 4-1 Illustration of Instability Point Determination

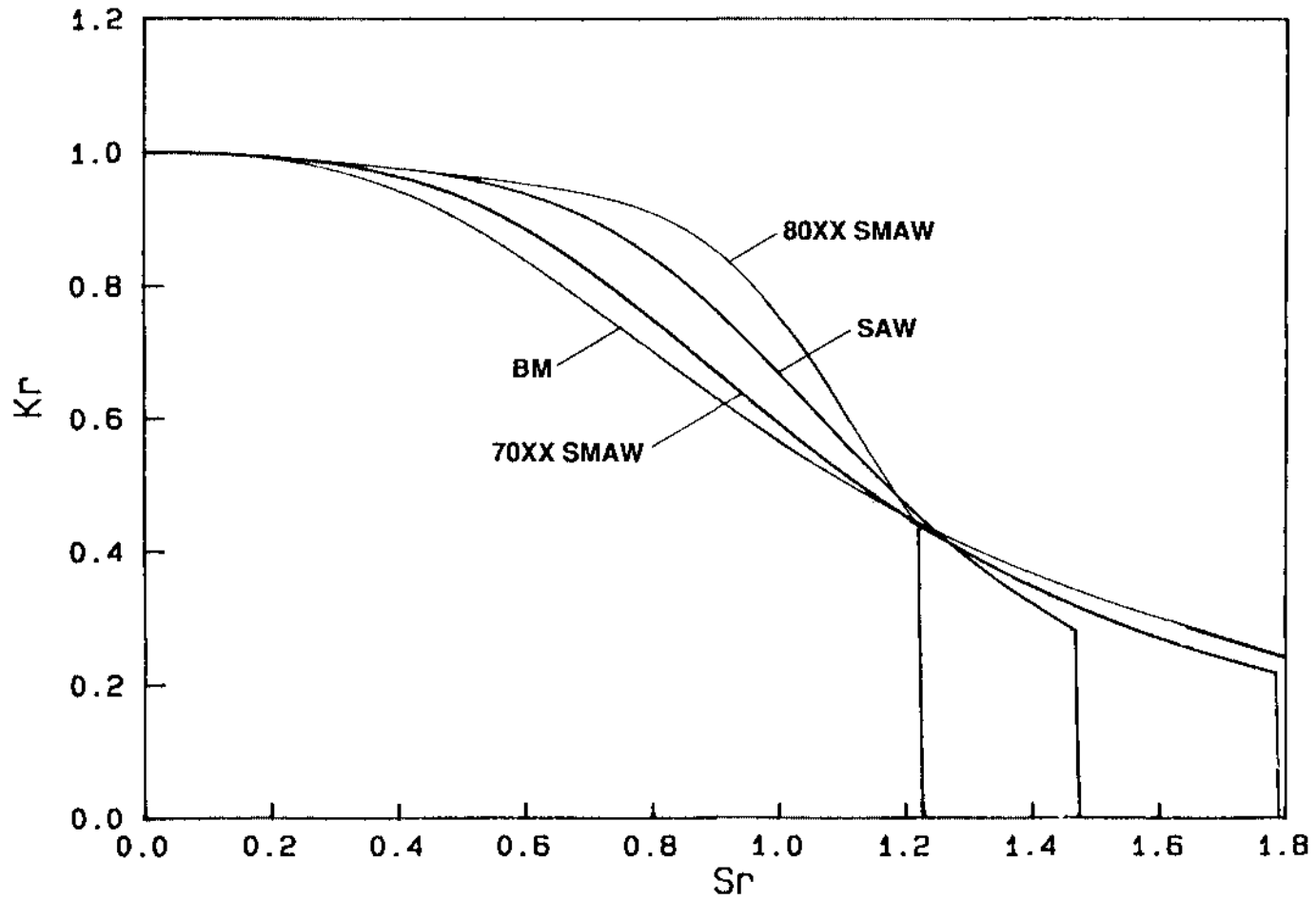


Figure 4-2 Comparison of Ferritic Material Categories for Axisymmetric Flaw for $a/t = 0.5$ and $R/t = 10$

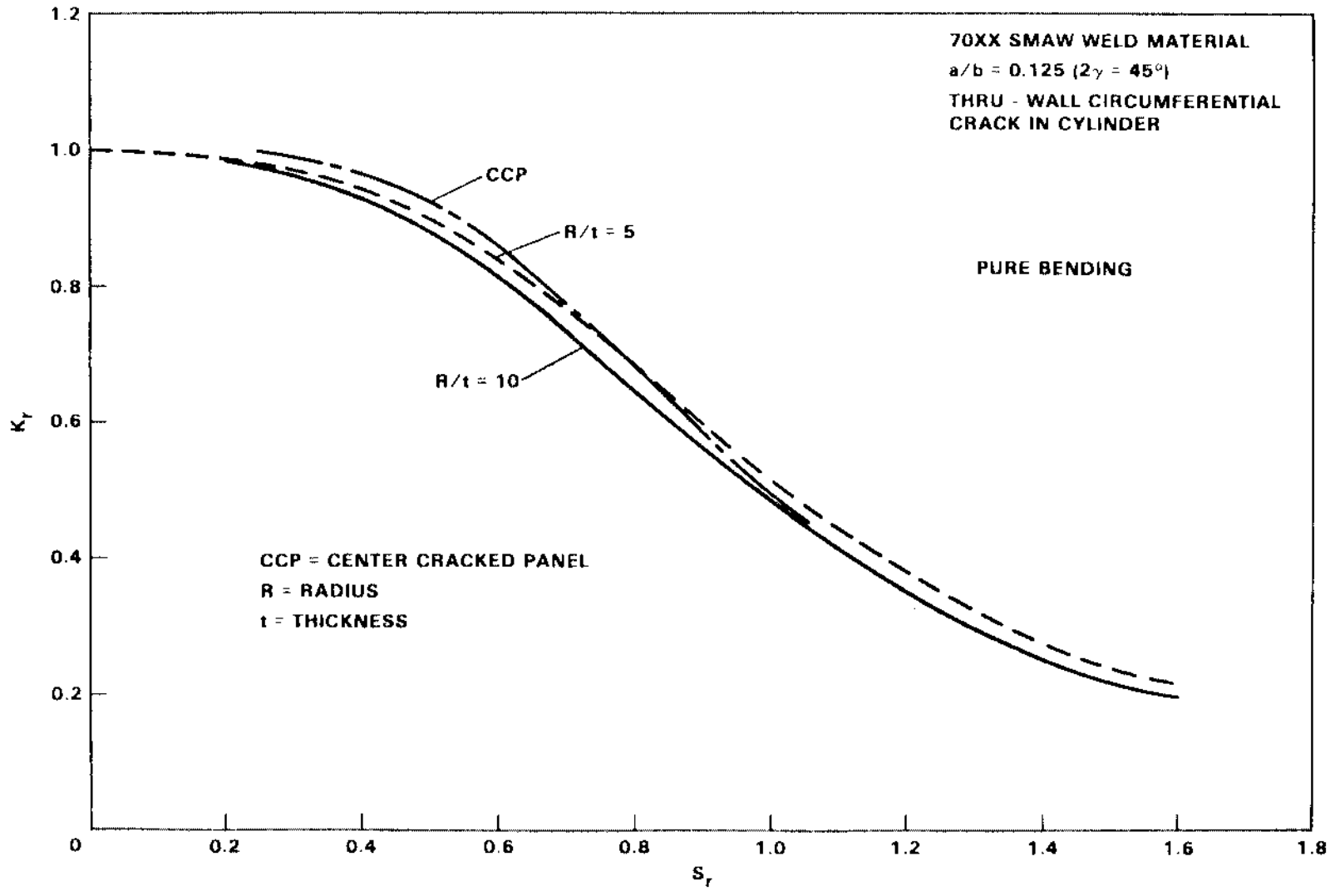


Figure 4-3 Comparison of R/t Effects on DPFAD Curves for Through-Wall Circumferential Flaw Under Pure Bending

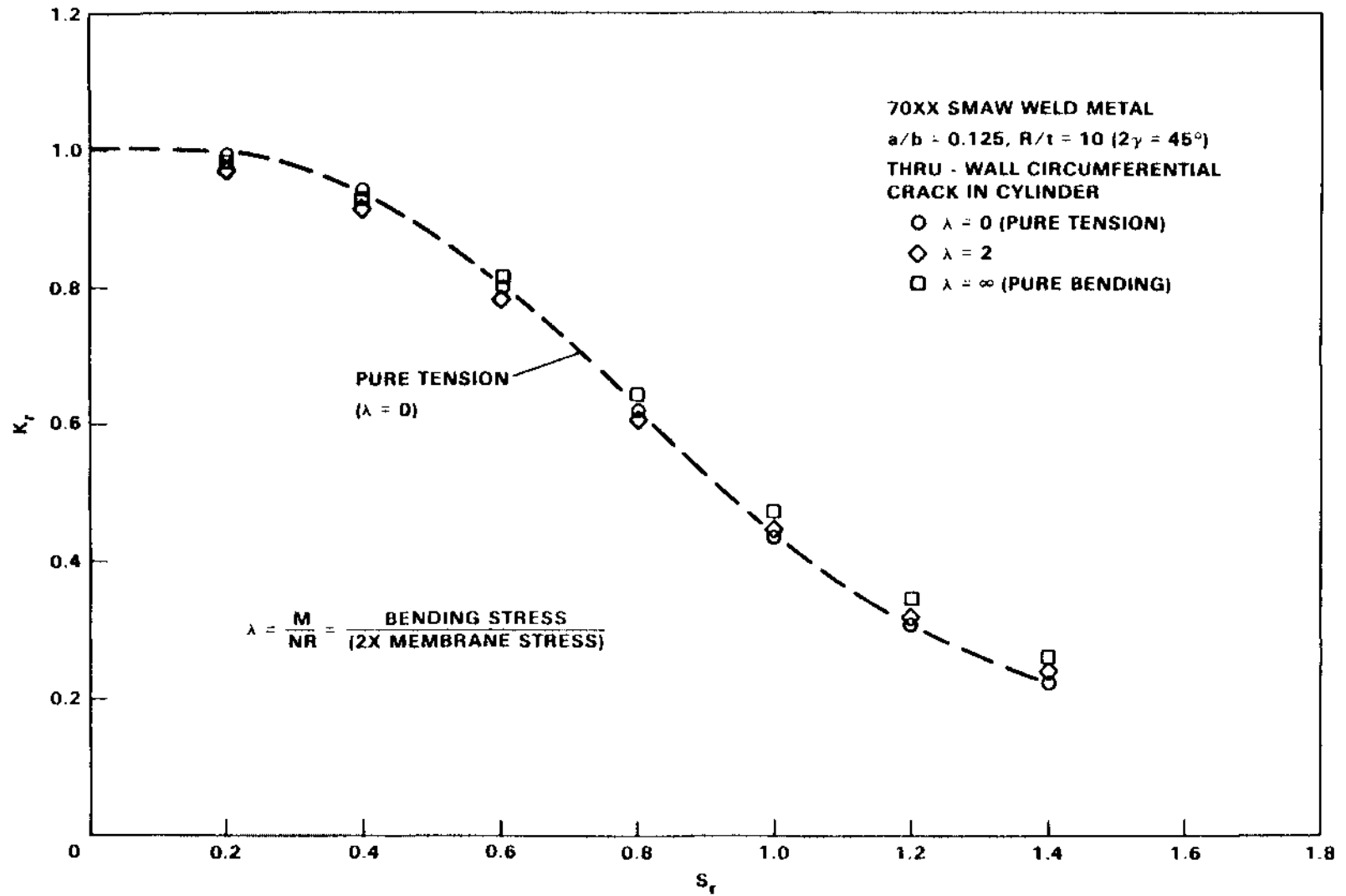


Figure 4-4 Comparison of Effects of Loading (Bending versus Tension) for Through-Wall Circumferential Flaw for 70XX SMAW Weld Metal

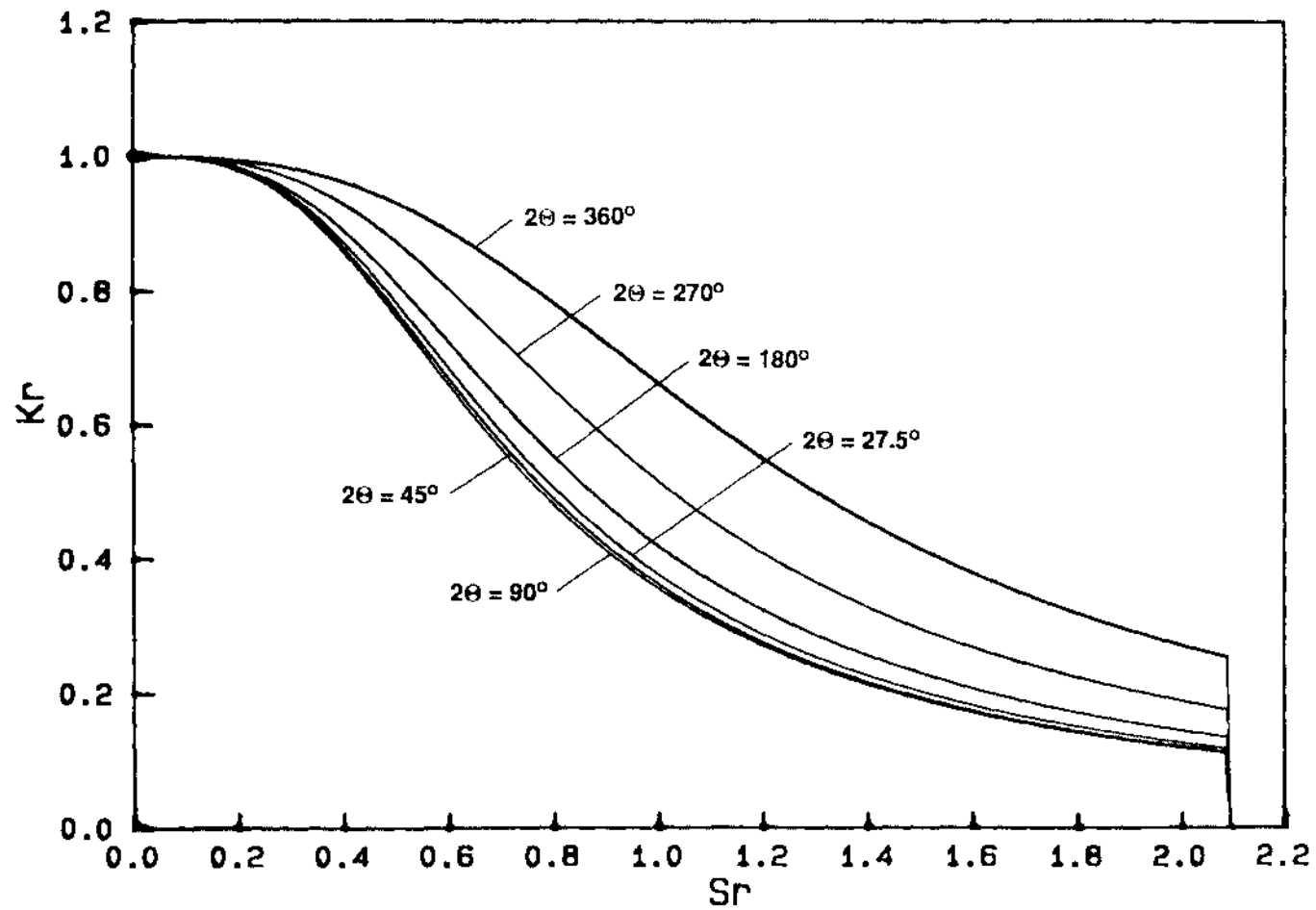


Figure 4-5 Comparison of θ Variation for Part Through-the-Wall Flaw in Pipe When Tensile Loading for $a/t = 0.5$ for Ferritic Base Metal

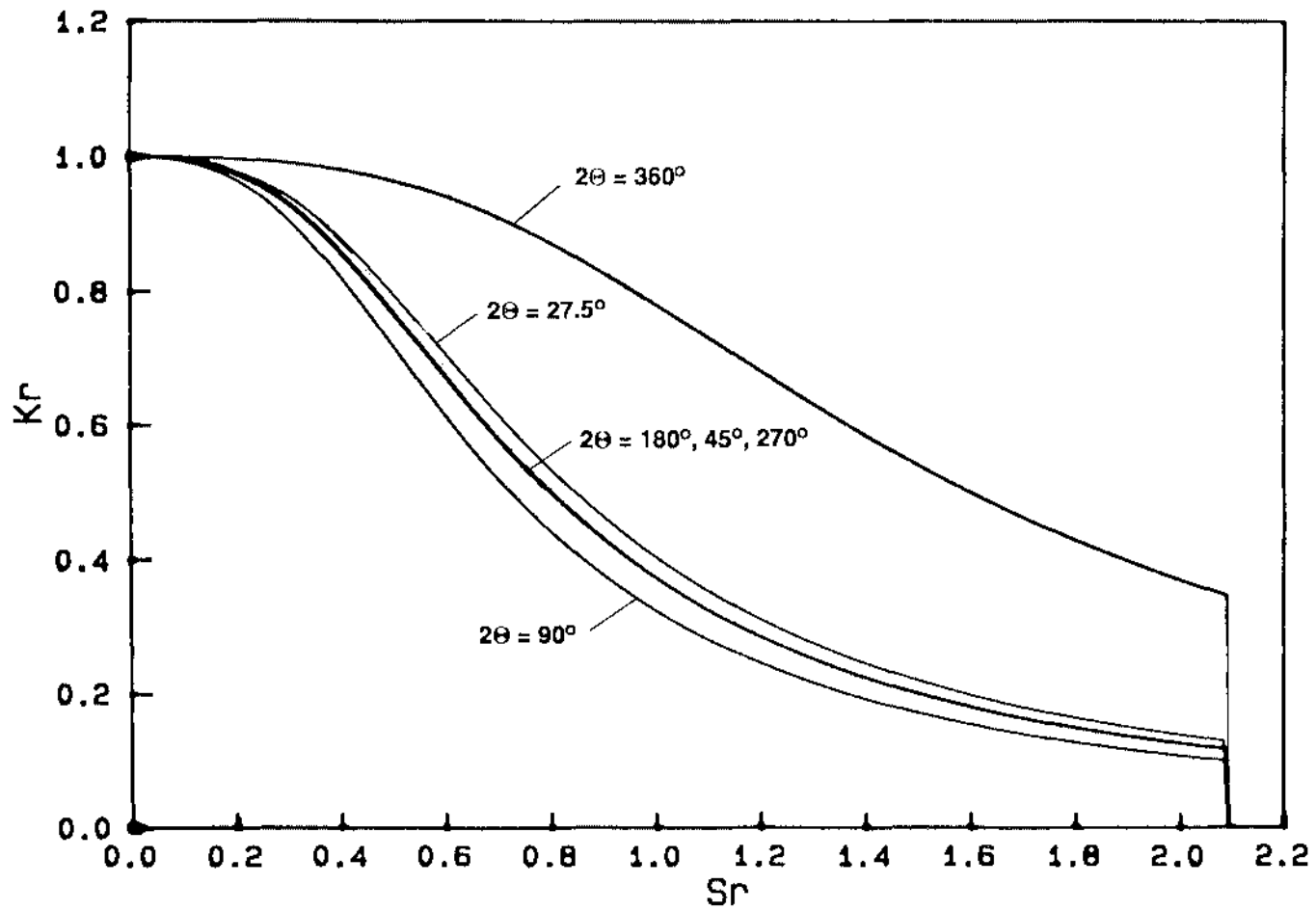


Figure 4.6 Comparison of θ Variation for Part Through-the-Wall Flaw in Pipe Under Tensile Loading for $a/t = 0.75$ for Ferritic Base Material

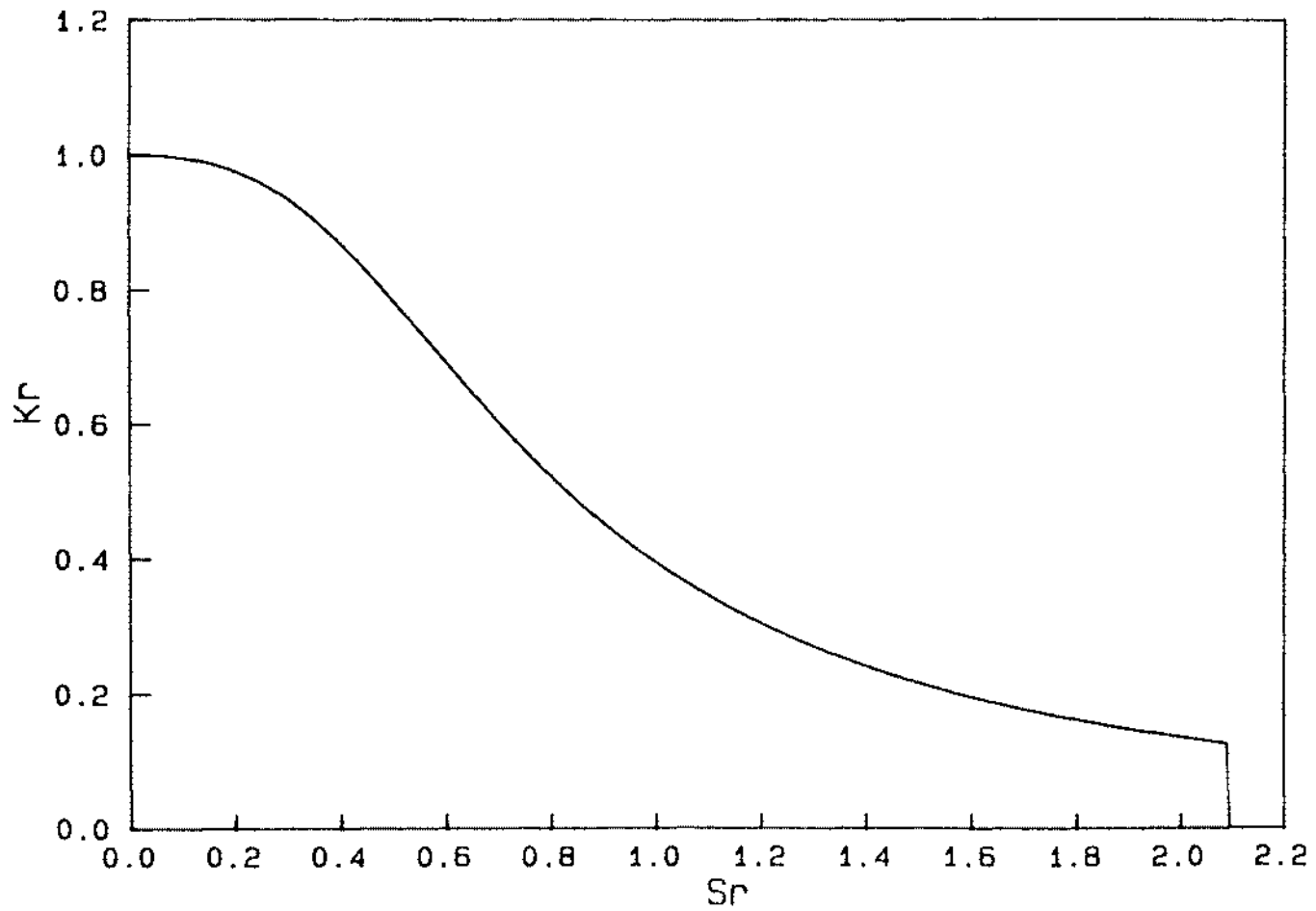


Figure 4-7 DFFAD Curve for Part-Through-the-Wall Flaw $\theta = 45$ degrees
for Pipe Under Bending for $a/t = 0.5$ for Ferritic Base Metal

Section 5

VALIDATION OF SIMPLIFIED APPROACH

The validation of the simplified DPFAD approach for ferritic piping was accomplished through comparison of predicted failure loads using the DPFAD single curve for circumferential flaws and multiple curves (2) for axial flaws to the actual experimental failure loads for three sets of pipe experiments.

CIRCUMFERENTIAL FLAWS

The Battelle Columbus Laboratories (BCL) degraded piping program (Phase II) test results from (18) are summarized in Table 5-1 for part-through-the-wall flawed ferritic pipes under pure bending ($P_m = 0$) as well as experiment 4131-4 under combined tension plus bending where internal pressure was held constant, producing $P_m = 10.2$ ksi. Table 5-2 summarizes the JAERI test results (19) for Japanese tests of ferritic piping under pure bending. Lastly, Eiber/BCL (20) axial flawed pipe burst tests under pressure are summarized in Table 5-3. Plots produced using the Babcock & Wilcox computer code PCFAD (12) for each test were based on the actual failure pressures as input. The radial distances from the origin of the diagram to the assessment points (candy-canes) to the corresponding point of the failure assessment curve is a measure of the conservatism of the simplified DPFAD approach. The instability stress is the point which is connected with the line (dash-dot in Figure 5-1 for specimen BCL 4112-9) from the origin to the failure assessment curve. The appropriate ratios along these lines give the P_{bexp}/P_{bcal} ratios in the Tables. Table 5-1 presents the BCL (CSC) test predictions using actual BCL (21) compact test data (non-side grooved J_M^* resistance curves). The J_m^* is defined by BCL as the expected to be recommended ASTM E-24 J_R curve test procedure where J is separated into elastic and plastic components. It was noted that there was little difference between J_M^* and J_M for the ranges of the J_R curves used in the predictions. In addition to using the actual material J_R curves, the actual yield and ultimate strengths were used for calculating pipe specific "a" and "n" values in the generation of the DPFAD curve using PCFAD. The pipe specific

DPFAD curves are only slightly different from the lower bound generic ferritic base metal curve using $\alpha = 2.51$ and $n = 4.2$. The effect of using the non-generic α, n values is approximately .1% while the degree of conservatism in the predictions varies from +45% to +7%. Note that the DPFAD approach should always be somewhat conservative as the DPFAD curve reflects the initiation flaw size. For ductile tearing, these DPFAD curves would move outward from the origin a slight amount depending on how much ductile tearing occurs before instability. Further discussion can be found in (5). In Table 5-2, the JAERI tests were predicted using J_{IC} as resistance curves were not available. Note the consistency of the predictions in Table 5-2 for P_{bexp}/P_{bcal} from 1.28 to 1.39. Use of actual resistance curves would bring these ratios closer to 1.0 (less conservative).

AXIAL FLAWS

Limited test data was available for axial flaws in ferritic piping. The available pipe tests were done by Battelle Columbus Laboratories (BCL) in the early 1970's (20) under AEC sponsorship. Four axial flawed pipes under pressure (burst tests) in Table 5-3 were predicted using pipe material "representative" of CL oriented material with toughness of $J_{IC} = 277$ lb/in. The J_R curve used was the lower bound of all piping material (A106B) tested by Material Engineering Associates (MEA) taken from (3). Actual toughness measurements were not determined by BCL at the time of the AEC designated pipe tests. The only measure of toughness reported was Charpy energy values of from 50 to 60 ft-lbs at the test temperatures. The failure assessment point equations had to be adjusted to account for the external axial flaws of the AEC pipe tests. With the adjustment in the K_I and limit load equations, DPFAD predicted failure pressures due to ductile crack growth were from 28% nonconservative for pipe AEC-8 to 12% conservative for pipe AEC-19 with an average prediction of 1% nonconservative. Figure 5-2 presents the DPFAD plot for specimen AEC-20 where the predicted failure pressure was within 1% of the experimental burst pressure. For test specimen AEC-8 the prediction was 28% nonconservative. On examination of Figure 5-3 for the AEC-8 pipe it is observed that the failure mode is close to ultimate strength limit load (the intersection of the dash-dot line with the vertical line, $S_T = 2.34$). If the limit load is defined by the flow stress equal to the average of yield and ultimate strengths, the new cutoff would be at $S_T = 1.58$ and the predicted failure pressure would be significantly reduced and near the actual failure

pressure given in Table 5-3. Two additional pipe experiments, AEC-4 and AEC-9 not reported in Table 5-3 displayed similar limit load behavior at failure when plotted in DPFAD space. Additional details of the axial flawed pipe experiments can be found in (17).

Table 5-1

BCL Tests (CSC)
Predictions Using Actual Material Properties

<u>EXP. NUMBER</u>	<u>4112-5</u>	<u>4112-6</u>	<u>4112-7</u>	<u>4112-8</u>	<u>4112-9</u>	<u>4115-1</u>	<u>4131-8</u>	<u>4131-4</u>
J_R Curve ¹	F1-ZP13-3LC	F30-ZP15-3LC	ZP14-3LC	F29-17	F-13-19	F-9-17	F-9-17	F-9-17
σ_Y (ksi)	30.8	46.4	37.5	34.4	38	34.7	34.7	34.7
σ_u (ksi)	67.8	90.0	82.7	88.5	88.7	76.5	76.5	76.5
σ_u/σ_Y^2	2.20	1.94	2.21	2.57	2.33	2.21	2.21	2.21
P_{bexp} (ksi)	36.7	43.4	47.5	36.8	34.5	38.3	36.5	27.0 10.2 ³
P_{bcal} (ksi)	33.5	31.5	32.9	26.0	32.1	31.3	30.7	23.7 9.0 ³
P_{bexp}/P_{bcal}	1.10	1.38	1.45	1.41	1.07	1.22	1.19	1.14

¹ Refers to BCL specimen ID number, all J_R curves from non-side grooved specimens. J_M or J_M used in analysis.

² DPFAD cutoff based on ultimate strength divided by yield strength.

³ Membrane stress.

Table 5-2
JAERI Tests (CSC)

<u>EXP. NUMBER</u>	<u>CS-11</u>	<u>CS-12</u>	<u>CS-13</u>	<u>CS-15</u>	<u>CS-16</u>
J_{IC}^1 (lb/in)	2016	2016	2016	2016	2016
σ_y (ksi) ²	35.6	35.6	35.6	35.6	35.6
P_{bexp} (ksi)	80.3	66.2	51.4	69.8	58.6
P_{bcal} (ksi)	62.9	47.7	37.0	52.1	45.0
P_{bexp}/P_{bcal}	1.28	1.39	1.39	1.34	1.30

¹ All JAERI test predictions based on initiation J_{IC} toughness.

² DPFAD cutoff based on $\sigma_u = 65$ ksi and σ_u/σ_y value.

Table 5-3
EIBER/BCL Axial Flawed Pipe Burst Tests

<u>EXPERIMENT NUMBER</u>	<u>AEC-8</u>	<u>AEC-18</u>	<u>AEC-19</u>	<u>AEC-20</u>
Material ¹	A106B	A106B	A106B	A106B
Yield Strength (ksi)	31.6	34.8	33.6	37.6
a/t	0.738	0.507	0.649	0.513
a/l	0.0518	0.0346	0.0905	0.0667
Test Temp. (°F)	696	469	628	504
Test Pressure at Failure (psig)	2300	1620	4300	1960
Pressure at Instability DPFAD (psig)	3147	1744	3812	1944
P_{exp}/P_{cal}	0.73	0.93	1.13	1.01

¹Material toughness taken from pipe tests for CL orientation at 550°F representative of material with toughness of $J_{IC} = 277$ lb/in; J_R curve used from MEA specimen ZP13-1CL (lowest J_R curve).

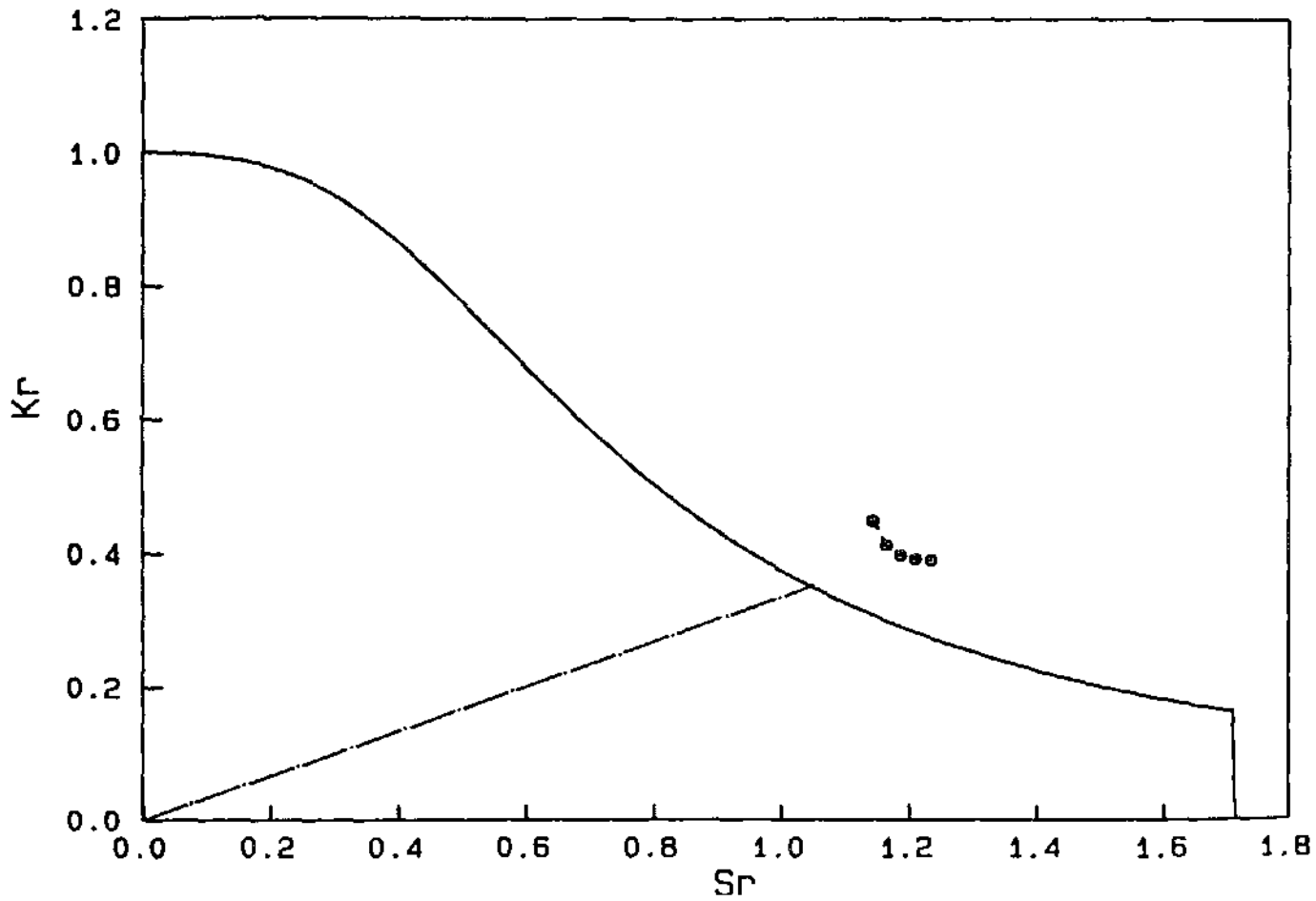


Figure 5-1 Failure Loading Locus per J_R Resistance Curve
 Plotted in DPFAD Space for BCL Pipe Test 4112-9

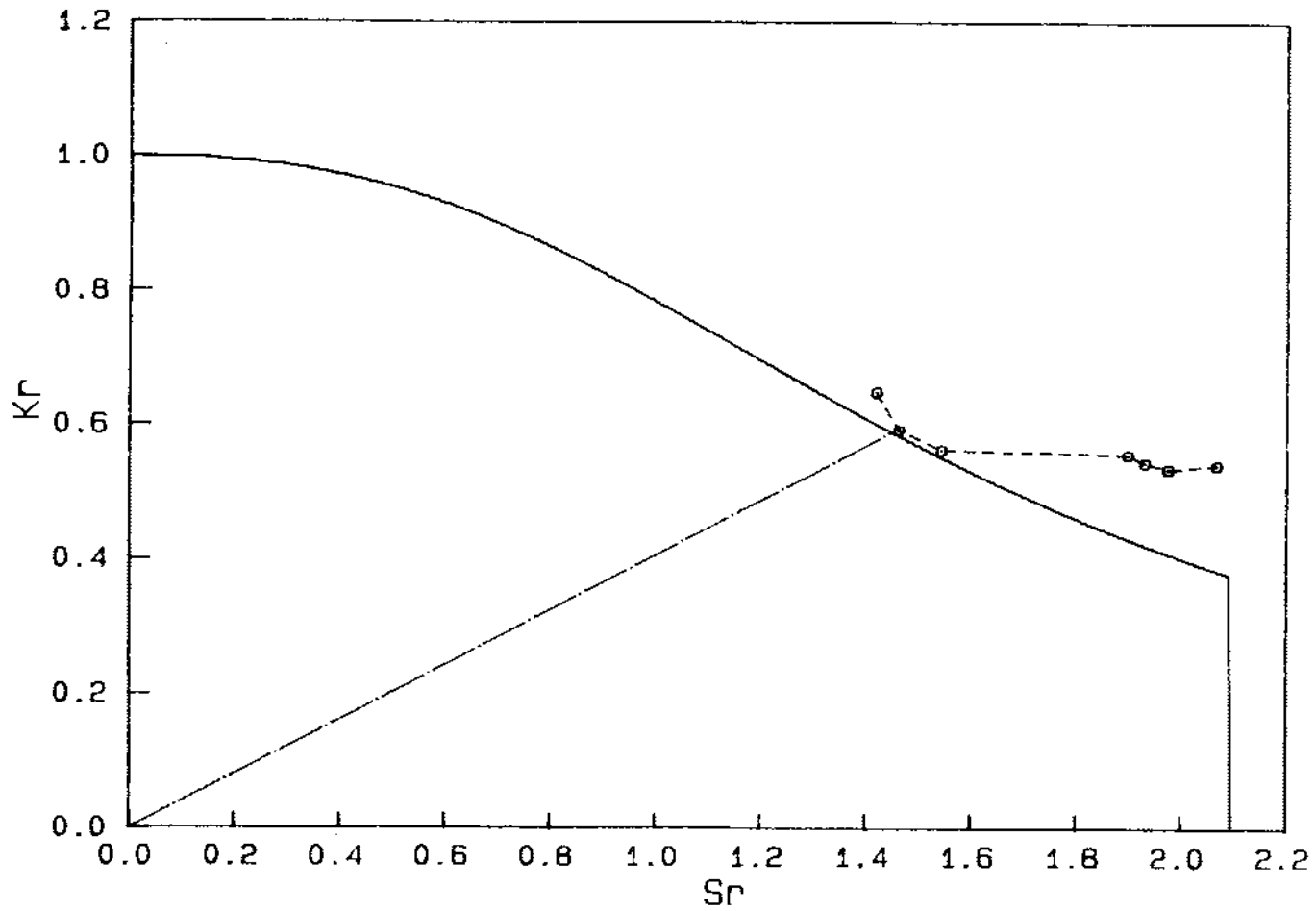


Figure 5-2 Failure Pressure Locus for J_R Resistance Curve
Plotted in DPFAD Space for AEC 20 Pipe Test

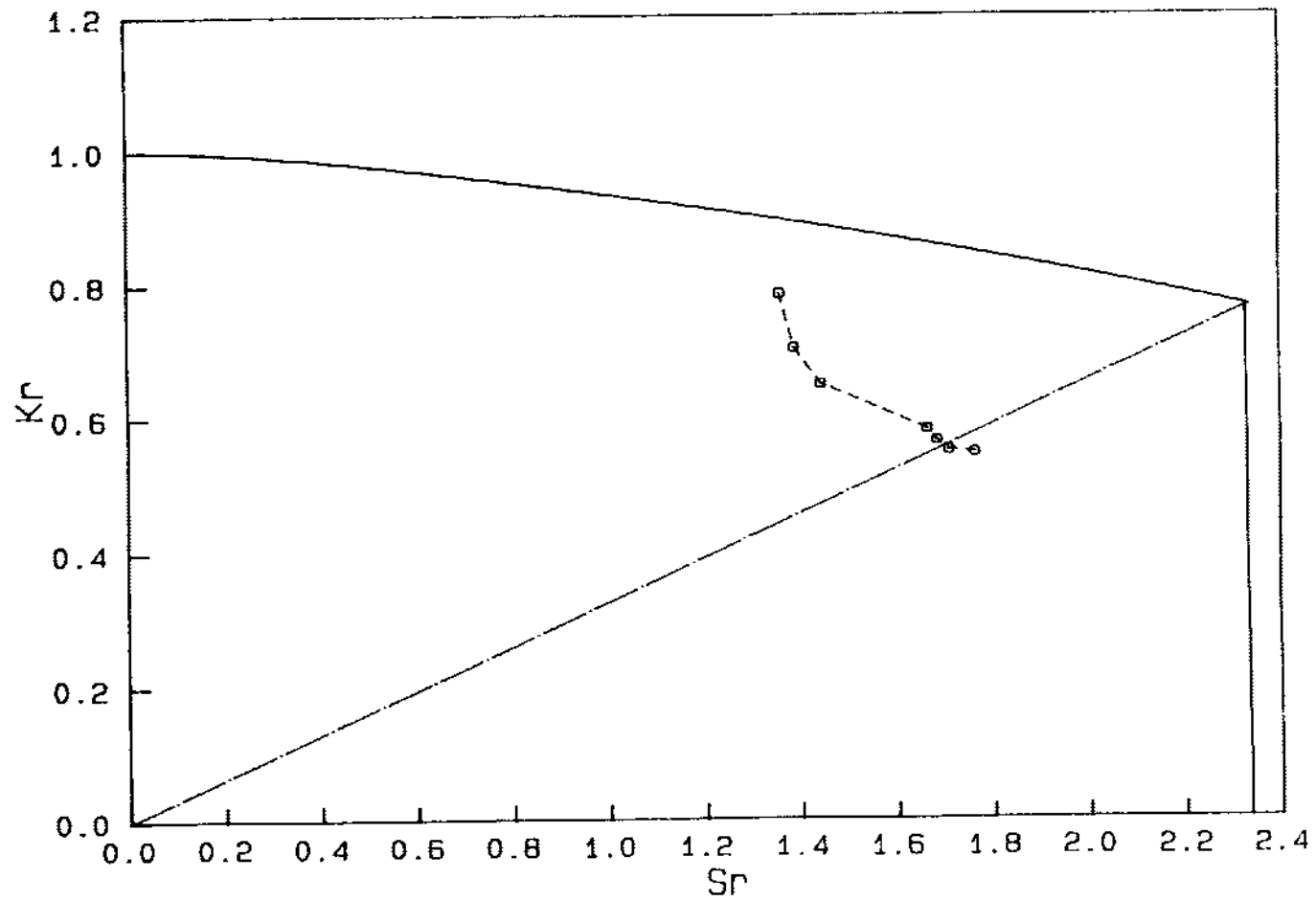


Figure 5-3 Failure Pressure Locus per J_R Resistance Curve
Plotted in DPFAD Space for AEC 8 Pipe Test

Section 6

CONCLUSIONS

A simple procedure for the evaluation of the acceptability of flaws detected in ferritic piping using the DPFAD methodology has been discussed. It has been shown that the general DPFAD approach for flawed ferritic piping can be reduced to one DPFAD curve for the assessment of part-through-the-wall circumferential flaws and two DPFAD curves for the assessment of part-through-the-wall axial flaws. Validation of the simplified approach has been demonstrated through comparisons with actual experimental test results of degraded nuclear piping. The advantages of Appendix J through the direct use of the DPFAD methodology over Appendix Z in Code Case N-463 has been discussed with regard to Appendix J's applicability to all combinations of membrane and bending stresses, handling of residual stresses in the elastic-plastic failure regime, generality of Appendix J in its use of actual pipe material toughness properties, and lastly the incorporation of published J-integral solutions for part-through-the-wall flawed geometries in the Appendix J procedures.

Section 7

REFERENCES

1. American Society of Mechanical Engineers Boiler and Pressure Vessel Code, 1989 Edition (and Addenda).
2. 10 CFR, Code of Federal Regulations Part 50, United States Government, January 1984.
3. "Evaluation of Flaws in Ferritic Piping," Electric Power Research Institute Final Report NP-6045, Palo Alto, CA, October 1988.
4. J. M. Bloom, "Validation of a Deformation Plasticity Failure Assessment Diagram Approach to Flaw Evaluation," in Elastic-Plastic Fracture: Second Symposium Volume II - Fracture Resistance Curves and Engineering Applications, ASTM STP 803, C. F. Shih and J. P. Gudas, eds., American Society for Testing and Materials, 1983, p. II-20-6 - II-238.
5. J. M. Bloom, "Deformation Plasticity Failure Assessment Diagram," Elastic-Plastic Fracture Mechanics Technology, ASTM STP 896, eds. J. C. Newman, Jr. and E. F. Loss, American Society for Testing and Materials, Philadelphia, 1985.
6. J. M. Bloom, "Simplified Procedures for Handling Self-Equilibrating Secondary Stresses in the Deformation Plasticity Failure Assessment Diagram Approach," Non-linear Fracture Mechanics, Volume II - Elastic-Plastic Fracture, ASTM STP 995, American Society for Testing and Materials, 1989, pp. 280-305.
7. V. Kumar, M. D. German, and C. F. Shih, "An Engineering Approach for Elastic-Plastic Fracture Analysis," Topical Report No. EPRI NP-1931, Research Project 1237-1, General Electric Company, Schenectady, NY, July 1981.
8. V. Kumar, M. D. German, W. W. Wilkening, W. R. Andrews, H. D. deLorenzi, and D. F. Mowbray, "Advances in Elastic-Plastic Fracture Analysis," EPRI Final Report No. NP-3607, Research Project 1237-1, General Electric Company, Schenectady, NY, August 1984.
9. I. Milne, R. A. Ainsworth, A. R. Dowling, and A. T. Stewart, "Assessment of the Integrity of Structures Containing Defects," CEGB Report No. R/H/R6-Rev. 3, Central Electricity Generating board, United Kingdom, 1986.
10. A. R. Dowling and C. H. A. Townley, "The Effects of Defects on Structural Failures: A Two-Criteria approach," International Journal of Pressure Vessels and Piping, Vol. 3, 1975, p. 77.

11. V. Kumar and M. D. German, "Elastic-Plastic Fracture Analysis of Through-Wall and Surface Flaws in Cylinders," EPRI Final Report NP-5596, Research Project 1237-5, General Electric Company, Schenectady, NY, January 1988.
12. J. M. Bloom, "User's Guide for the Failure Assessment Diagram -- Computer Code "FAD"," Babcock & Wilcox Report, Babcock & Wilcox Alliance Research Center, Revision 3a, October 1987.
13. A. Zahoor, R. M. Gamble, H. S. Mehta, S. Yukawa and S. Ranganath, "Evaluation of Flaws in Carbon Steel Piping," EPRI NP-4824M and NP-4824SP, October 1986.
14. J. M. Bloom and S. N. Malik, "A Procedure for the Assessment of the Integrity of Nuclear Pressure Vessels and Piping Containing Defects," EPRI Topical Report NP-2431, Research Project 1237-2, Electric Power Research Institute, Palo Alto, Calif., June 1982.
15. B. R. Ganta, D. J. Ayres and D. M. Norris, "Analysis of a Pipe Weldment with a Circumferential Through-Wall Crack," ASME PVP paper 87-PVP-34, presented at the Pressure Vessel and Piping Conference, San Diego, CA, June 28 - July 2, 1987.
16. J. M. Bloom, "Extensions of the Failure Assessment Diagram Approach Semi-Elliptical Flaw in Pressurized Cylinders - Part II," ASME Journal of Pressure Vessel Technology, November 1986, Vol. 108, p. 485.
17. J. M. Bloom, "Validation of the Deformation Plasticity Failure Assessment Diagram (DPPAD) Approach -- The Case of an Axial Flaw in a Pressurized Cylinder," presented at the Fracture Mechanics and Plasticity in Pressure Vessels Session, ASME Winter Annual Meeting, Chicago, Nov. 28 - Dec. 2, 1988. Submitted to ASME Journal of PVP, 1989.
18. G. M. Wilkowski, et al., "Degraded Piping Program Phase II," Semi-annual Report, October 1984 - March 1985, NUREG/CR-4082, BMI-2120, Vol. 2, July 1985.
19. D. M. Norris and K. Kishida, "Evaluation of Flaws in Nuclear Piping," presented at the SMIRT Conference held at Lausanne, Switzerland, Paper Number GF5/1, 1987.
20. R. Eiber, et al., "Investigations of the Initiation and Extent of Ductile Pipe Rupture," BMI-1980, Columbus, Ohio, June 1971.
21. C. W. Marshall, "Mechanical Property Data for Samples Machined from Six Different Carbon Steel Pipes," personal communication to J. Bloom, November 23, 1987.
22. I. Sprung and V. A. Zilberstein, "Fracture Mechanics Analysis of Welding Residual Stress Effects in ASME III Support Structures," presented at the 64th Annual Convention of the American Welding Society, Philadelphia, PA, April 24-29, 1983, TP 83-9.

Section 8

NOMENCLATURE

a	=	the general depth dimension for a flaw (inches)
a_f	=	the maximum depth to which the detected flaw is calculated to grow by the end of the evaluation period (inches)
E'	=	$E/(1-\nu^2)$ (ksi)
E	=	Young's modulus (ksi)
σ_{ys}	=	Yield strength (ksi)
J_{Ic}	=	measure of toughness due to crack extension at upper shelf, transition, and lower shelf temperatures (in-lbs/in ²)
l_{crit}	=	critical flaw length for stability of an axial through-the-wall flaw (inches)
σ_h	=	hoop stress in the pipe at the flaw (ksi)
t	=	pipe wall thickness (inches)
P_m	=	the primary membrane stress in the pipe at the flaw (ksi)
P_b	=	the primary bending stress in the pipe at the flaw (ksi)
P'_b	=	bending stress at collapse limit load for any combination of primary and expansion stress (ksi)
θ	=	one-half of the final flaw angle (see Figure 3-1) (radians)
ν	=	Poisson's ratio
β	=	angle to neutral axis of flawed pipe (radians)
(SF)	=	safety factor (dimensionless)
K_I	=	mode I stress intensity factor (ksi \sqrt{in})
P_e	=	pipe expansion stress (ksi)
F_m	=	parameter for circumferential flaw membrane stress intensity factor
F_b	=	parameter for circumferential flaw bending stress intensity factor

p	=	internal pressure (ksi)
R_1	=	inside radius of pipe (inches)
R_2	=	outside radius of pipe (inches)
Q	=	flaw shape parameter (dimensionless)
σ_0, ϵ_0	=	reference stress and strain as used in the Ramberg-Osgood equation (ksi, dimensionless)
G	=	total elastic energy available per unit increase in crack surface area (in lb/in ²)
J_{applied}	=	the J-integral structural response (in-lb/in ²)
J_p	=	plastic component of J_{applied} (in-lb/in ²)
α, n	=	Ramberg-Osgood parameters (dimensionless)
CL	=	orientation of a test specimen in the circumferential direction with longitudinal crack plane orientation
$J_R(\Delta a)$	=	Material's J-integral resistance to ductile tearing at a prescribed Δa value obtained from accepted test procedures (in-lbs/in ²)
Δa	=	amount of ductile flaw extension (inches)
P'_m	=	membrane stress at reference limit load for any combination of primary and expansion stresses (ksi)
K'_f	=	the brittle fracture component of the assessment point defined by the ratio of the stress intensity factor to the material fracture toughness (dimensionless)
K_r	=	the ordinate of the FAD curve (dimensionless)
S'_f	=	the limit load component of the assessment point defined for circumferential flaws by the ratio of the applied stress to the membrane stress at reference limit load (P'_m) and for axial flaws as the ratio of pressure to the reference limit (load) pressure (P_0) (dimensionless)
S_r	=	the abscissa of the FAD curve (dimensionless)
σ_f	=	the material's flow stress, equal to the average of the yield stress (σ_y) and the engineering ultimate stress (σ_u) (ksi)
σ_u	=	engineering ultimate stress (ksi)
$S_{r\text{cutoff}}$	=	maximum value of S_r at the vertical (limit load) boundary of the failure assessment diagram curve (dimensionless)
J^e_f	=	the elastic J-integral (in-lbs/in ²)

a'	=	sum of the flaw depth plus the amount of ductile flaw extension (inches)
P_0	=	reference limit (load) pressure (ksi)
Γ_m	=	factor in the reference limit load expressions reflecting the effect of flaw size (dimensionless)
γ	=	factor in the reference limit load expression for P'_m reflecting the ratio of P_b to P_m (dimensionless)
R_c	=	sum of the flaw depth and the inside radius of pipe (inches)
a^*	=	equivalent flaw depth for a part through-the-wall axial flaw in a pipe under internal pressure (inches)
F_1	=	total geometry correction factor for an interior axial part through-the-wall flaw in a pressurized pipe (dimensionless)
M_1, M_2, M_3	=	geometry correction factor for an interior axial part through-the-wall flaw in a pressurized pipe which accounts for the flaw aspect ratio, a/l (dimensionless)
f_c	=	geometry correction term which accounts for the flaw depth and wall thickness relative to the pipe inside radius (dimensionless)
R	=	mean radius of pipe (inches)
P_{m1}	=	membrane stress at collapse limit load with zero primary bending stress (ksi)
ψ	=	angle used in defining P_{m1} (radians)
l	=	general flaw length dimensions (inches)
x	=	dimensionless parameter a/t
σ_1	=	hoop stress at collapse limit load for an axial flaw (ksi)
M_2	=	parameter for collapse hoop stress (dimensionless)
J_e	=	the elastic J-integral calculated from the stress intensity factor K_I ($\text{in}\cdot\text{lb}/\text{in}^2$)
K_I^S	=	stress intensity factor due to residual stresses (ksi $\sqrt{\text{in}}$)
ρ	=	term used to correct K_I^S for the elastic-plastic effects of residual stresses (dimensionless)
R_y	=	radius of the plastic zone for plane stress conditions (inches)
$K_I^{S'}$	=	brittle component of the assessment point due to residual stresses (dimensionless)

TOTAL
 K'_r = sum of K'_r , K^S_r , and ρ (dimensionless)

Z = a measure of plasticity due to small scale yielding
(dimensionless)

Appendix A

FAILURE ASSESSMENT CURVES

The appropriate DPFAD curves developed for Appendix J as shown in Figures 2-1 and 2-2 were determined using Eq. 4-4 with $\alpha = 2.51$ and $n = 4.2$ determined from (1) as being the lower bound stress-strain Ramberg-Osgood fit for ferritic base metal.

CIRCUMFERENTIAL FLAWS

The single DPFAD curve for part-through-the-wall circumferential flaws was developed from a geometry of $a/t = 0.5$, $R/t = 10$ and $\theta = 90^\circ$ under axial loading for the lower bound α, n of a ferritic base metal. The equations for this failure assessment curve are given as follows:

$$\frac{1}{K_T^2} = \frac{J_{\text{applied}}}{J_e} = \frac{a_e}{a} \left[\frac{F_m(a_e)}{F_m(a)} \right]^2 + \frac{\alpha(1-a/t)h_1 S_r^{n-1}}{\pi \Gamma^2 F_m^2 / Q} \quad (\text{A-1})$$

where

$$\Gamma^2 = (0.95)^2 \left[(1-a/t) - .0525 (a/t)^2 + \frac{\pi-\theta}{\pi} (a/t) (1+0.0525 a/t) \right]^2 \quad (\text{A-2})$$

and

$$F_m = 1.0 + \{0.02 + \alpha' (0.0103 + 0.00617\alpha') + 0.0108 (1-0.7\alpha')\} \cdot Q^2 \quad (\text{A-3})$$

and

$$Q = 1 + 1.464 (2a/l)^{1.65} \quad (\text{A-4})$$

$$\alpha' = (a/t) (2a/l) \approx 20 \cdot \theta \text{ for } R/t = 10 \quad (\text{A-5})$$

$$a_e/a = 1.0 + \frac{\Gamma^2 F_m^2}{6Q} \left[\frac{S_r^2}{(1+S_r^2)} \right] \left(\frac{n-1}{n+1} \right) \quad (\text{A-6})$$

$$S_r = \sigma_m / (\sigma_y \Gamma) \quad (A-7)$$

The value of h_1 is 29.1 found from interpolating the values from (2). Table A-1 gives the coordinates (K_r, S_r) of the failure assessment curve of Figure 2-1.

AXIAL FLAWS

The two DPFAD curves to be used for evaluation of part-through-the-wall axial flaws are based on continuous internal axial flaws for $a/t = 1/8$ and $5/8$ with $R_i/t = 10$ under internal pressure for the lower bound α, n of a ferritic base metal as discussed in Section 4.5. The equations for these failure assessment curves are given as follows:

$$\frac{1}{K_r^2} = \frac{J_{\text{applied}}}{J_e} = \frac{a_e}{a} \left[\frac{F_1(a_e)}{F_1(a)} \right]^2 + \frac{\alpha(1-a/t)h_1 S_r^{n-1}}{3.846 F_1^2 \Gamma^2} \quad (A-8)$$

where

$$\Gamma = \frac{(1-a/t)}{(1+0.1a/t)} \quad (A-9)$$

and

$$F_1 = \frac{1.165 - 1.339 a/t}{(1-a/t)^{5/2}} \quad (A-10)$$

for the range of $1/8 \leq a/t \leq 3/4$

$$a_e/a = 1 + 0.222 \left(\frac{n-1}{n+1} \right) \frac{F_1^2 \Gamma^2 S_r^2}{(1+S_r^2)} \quad (A-11)$$

$$S_r = \frac{P}{P_0} \quad \text{where} \quad P_0 = \frac{2 \sigma_y (1-a/t)}{10\sqrt{3} (1+0.1a/t)} \quad (A-12)$$

The value of h_1 is 8.29 for $a/t = 1/8$ and 5.29 for $a/t = 5/8$ obtained from interpolation of the values for h_1 found in (3) for $\alpha = 2.51$ and $n = 4.2$. Table A-2 gives the coordinates (K_r, S_r) of the failure assessment curves shown in Figure 2-2.

Appendix A

References

- A-1 "Evaluation of Flaws in Ferritic Piping," Electric Power Research Institute Final Report NP-6045, Palo Alto, CA, October 1988.
- A-2 V. Kumar and M. D. German, "Elastic-Plastic Fracture Analysis of Through-Wall and Surface Flaws in Cylinders," EPRI Final Report NP-5596, Research Project 1237-5, General Electric Company, Schenectady, NY, January 1988.
- A-3 V. Kumar, M. D. German, and C. F. Shih, "An Engineering Approach for Elastic-Plastic Fracture Analysis," Topical Report No. EPRI NP-1931, Research Project 1237-1, General Electric Company, Schenectady, NY, July 1981.

TABLE A-1

DPFAD COORDINATES (K_r, S_r) FOR
PART-THROUGH-THE-WALL CIRCUMFERENTIAL FLAWS
IN FERRITIC PIPING

K_r	S_r
1.000	0.000
0.996	0.100
0.975	0.200
0.927	0.300
0.850	0.400
0.757	0.500
0.660	0.600
0.570	0.700
0.492	0.800
0.426	0.900
0.371	1.000
0.326	1.100
0.288	1.200
0.256	1.300
0.229	1.400
0.207	1.500

TABLE A-2

DPFAD COORDINATES (K_r, S_r) FOR
PART-THROUGH-WALL AXIAL FLAWS
IN FERRITIC PIPING

$0.125 \leq a/t \leq 0.25$ $0.50 \leq a/t \leq 0.75$

K_r	K_r	S_r
1.000	1.000	0.000
0.998	0.995	0.100
0.985	0.978	0.200
0.957	0.951	0.300
0.908	0.915	0.400
0.841	0.873	0.500
0.763	0.828	0.600
0.683	0.781	0.700
0.606	0.735	0.800
0.536	0.690	0.900
0.475	0.647	1.000
0.422	0.605	1.100
0.376	0.567	1.200
0.337	0.530	1.300
0.303	0.496	1.400
0.275	0.464	1.500

Appendix B

LIMIT LOAD - S_f^{cutoff}

An upper-bound limit on the coordinate S_f^{cutoff} is drawn as a vertical line on the failure assessment diagram as a restriction against plastic collapse, as discussed in Section 4-6. This limit, in general, applies to primary stresses only. Plastic collapse is assumed to occur when the remaining ligament of the flawed section of the pipe becomes fully plastic prior to flaw instability due to flaw extension. This criterion implies that the flawed pipe is at the point of incipient failure when the net section in the flaw plane first forms a plastic hinge. Failure is assumed to occur at a critical flow stress, σ_f , which is defined from material strength properties. The flow stress is taken to be the average of the 0.2% offset yield stress and engineering ultimate stress.

The procedures developed in this appendix are intended to produce results for the limit load flaw evaluation methodology which are consistent with the procedures given in the ASME Section XI, Code Case N-463-1 (1).

LIMIT LOAD CUTOFF FOR CIRCUMFERENTIAL FLAWS

The flaw evaluation procedure for the plastic collapse failure mode is based on earlier work by Kanninen, et al. (2,3), and follows the procedure previously used by the ASME Section XI Working Group on Flaw Evaluation for austenitic (4) and ferritic (5) steel piping. The relationship between the collapse load and flaw size is obtained by requiring force and moment equilibrium of the pipe section. The flaw depth, a , and half angle, θ , at plastic collapse is determined from the following equations.

For flaws which do not penetrate the compressive region of the pipe,

$$\theta + \beta \leq \pi,$$

$$\sigma_b = (2\sigma_f/\pi)[2\sin\beta - (a/t)\sin\theta]$$

$$\beta = 0.5\pi[1 - (a/t)(\theta/\pi) - \sigma_m/\sigma_f] \quad (B-1)$$

and for flaws which penetrate the compressive region of the pipe, $\theta + \beta > \pi$,

$$\sigma_b = (2\sigma_f/\pi) [2 - (a/t)]\sin\beta$$

$$\beta = \frac{\pi [1 - (a/t) - \sigma_m/\sigma_f]}{(2 - (a/t))} \quad (B-2)$$

Here σ_m and σ_b are the primary membrane and bending stresses, respectively, corresponding to plastic collapse for any specified flaw depth and angle, and σ_f is the flow stress.

For combined membrane and bending stresses the failure assessment coordinate S'_r is given by

$$S'_r = SF P_m/P'_m(\hat{a}) \quad (B-3)$$

where SF is the required safety factor on stress, P_m is the actual primary membrane stress, $P'_m(\hat{a})$ is the primary membrane stress at reference limit load given by

$$P'_m(\hat{a}) = \sigma_y \gamma \Gamma_m(\hat{a}) \quad (B-4)$$

where σ_y is the yield stress and $\Gamma_m(\hat{a})$ is calculated for a flaw depth which has been updated by the ductile flaw extension Δa ,

$$\hat{a} = a + \Delta a \quad (B-5)$$

where a is the flaw depth prior to ductile flaw extension.

The other terms are given by

$$\gamma = -\frac{\pi P_b}{8P_m} + \left[\left(\frac{\pi P_b}{8P_m} \right)^2 + 1 \right]^{0.5} \quad (B-6)$$

$$\Gamma_m(\hat{a}) = \frac{[R_2^2 - R_c^2 + (1 - \theta/\pi)(R_c^2 - R_1^2)]}{(R_2^2 - R_1^2)} \quad (B-7)$$

$$R_c = R_1 + \acute{a}, \quad (B-8)$$

and R_1 and R_2 are the inner and outer radii of the pipe, respectively.

The limit load bound for combined stresses is written in terms of a bending stress,

$$SF S_c = \sigma_b(a) \quad (B-9)$$

where S_c is the allowable primary bending stress and $\sigma_b(a)$ is the primary bending stress at limit load evaluated from equation (B-1) or (B-2) with the initial flaw depth a , which has not been updated for ductile flaw extension.

In the flaw evaluation procedures in the Code Case N-463-1 (1), the limit load methodology is used after the screening criterion has determined that the mode of failure would be plastic collapse. The flaw depth used in the procedures in (1,5) is therefore the flaw depth with no prior ductile flaw extension. However, in the failure assessment diagram approach used here the reference limit load (Eq.B-4) is updated with ductile flaw extension in calculating the coordinate S'_r . In the FAD approach (6,7) the limit on plastic collapse is in general implicitly based on the updated flaw depth. For expediency the limit load cutoff given here is evaluated based on the initial flaw depth a , on the basis that this is a good approximation for small amounts of flaw extension.

To enforce this limit load bound on the abscissa of the failure assessment diagram, which in this case is based on membrane stress, Eq. B-9 is written in terms of a membrane stress. For this purpose the primary membrane and bending stresses are treated as increasing in a proportional fashion.

$$P_b/P_m = \text{constant} \quad (B-10)$$

Eq. B-3 is then written as

$$S'_r = SF P_b(P_m/P_b)/P'_m(\acute{a}) \quad (B-11)$$

Upon comparing equations (B-9) and (B-11), the limit load cutoff, $S'_r{}^{\text{cutoff}}$, given by the limit load bound $P_b = S_c$, is given by

$$S'_r{}^{\text{cutoff}} = (\sigma_b(a)/P'_m(\acute{a}))(P_m/P_b) \quad (B-12)$$

where for expediency the initial flaw depth, a , has been substituted in place of the updated flaw depth, \hat{a} , in evaluating P_m' .

Application of the Safety Factor

By assuming proportional loading (Eq. B-10), Eq. B-1 or B-2 can be solved for the primary membrane stress, σ_m , and primary bending stress, σ_b , at limit load. The allowable primary bending stress, S_c , and therefore the limit load cutoff, S_F^{cutoff} , could be determined in a consistent fashion with equal safety factors on P_m and P_b . However, Eqs. B-1 and B-2 are non-linear and σ_m , σ_b must be calculated by using an iterative technique. A simpler direct approach to calculating σ_b (and S_c) was adopted. The actual primary membrane stress, P_m , multiplied by the required safety factor on stress, SF, is substituted in place of σ_m in Eqs. B-1 and B-2 with the result:

for $\theta + \beta \leq \pi$

$$\sigma_b = (2\sigma_f/\pi)[2\sin\beta - (a/t)\sin\theta]$$

$$\beta = 0.5\pi[1 - (a/t)(\theta/\pi) - SF P_m/\sigma_f] \quad (\text{B-13})$$

and for $\theta + \beta > \pi$

$$\sigma_b = (2\sigma_f/\pi) [2 - (a/t)]\sin\beta$$

$$\beta = \frac{\pi}{(2 - (a/t))} [1 - (a/t) - SF P_m/\sigma_f] \quad (\text{B-14})$$

Eqs. B-13 and B-14 are used to provide a direct calculation of σ_b and therefore S_F^{cutoff} .

In calculating σ_b , and therefore S_c , the full safety factor, SF, is therefore applied to P_m ($\sigma_m = SF P_m$). This approach differs from the procedure given (1), in which the full safety factor is not applied to P_m . A comparison of the two procedures is given in Section B-1.3.

If the value of the primary bending stress at limit load, σ_b , is very small or negative, the limit load based on primary membrane stress alone has been reached or exceeded.

The approximate treatment of the primary membrane stress at limit load in calculating σ_b has the following implications:

- a) If the actual uniform safety margin on P_m and P_b equals the required safety factor, SF, the direct approach for calculating S_r^{cutoff} , will produce the same result as the consistent iterative method.
- b) If the actual uniform safety margin is less than the required safety factor, the direct approach will produce a value for S_r^{cutoff} which is lower than that from the consistent iterative approach. However, since the safety margin is less than the required safety factor, the failure assessment point would fall to the right of the consistent value of S_r^{cutoff} . The use of the direct-approach S_r^{cutoff} results in the failure assessment point lying further to the right of the S_r^{cutoff} than it would using the consistent value of S_r^{cutoff} . In either case the flaw would not meet the safety factor criterion.
- c) If the actual uniform safety margin is greater than the required safety factor, the direct approach will produce a value for S_r^{cutoff} which is higher than the consistent value. However, since the safety margin is greater than the required safety factor, the failure assessment point would fall to the left of the consistent value of S_r^{cutoff} . The use of the direct approach S_r^{cutoff} results in the failure assessment point lying further to the left of the S_r^{cutoff} than it would using the consistent value of S_r^{cutoff} . In either case the flaw would meet the safety factor criterion.

Primary Bending Stress With Zero Primary Membrane Stress

The limit load bound is given by Eq. B-9, where in this case the primary bending stress at limit load, $\sigma_b(a)$, is calculated by using Eq. B-13 or B-14 with $P_m = 0$. $\sigma_b(a)$ is calculated by using the initial flaw depth, a , prior to any ductile flaw extension.

For a primary membrane stress of zero the failure assessment coordinate S_r' is given by

$$S_r' = (\pi/4)SF P_b / (\sigma_y \Gamma_m(a)) \quad (\text{B-15})$$

where $\Gamma_m(a)$ is calculated by using Eqs. B-6 to B-8 with a flaw depth, a , updated with ductile flaw extension. By comparing Eqs. B-9 and B-15, the limit load cutoff, S_r^{cutoff} , given by the limit load bound $P_b = S_C$, and is written as

$$S_r^{\text{cutoff}} = (\pi/4)\sigma_b(a) / (\sigma_y \Gamma_m(a)) \quad (\text{B-16})$$

where the initial flaw depth, a , has been substituted in place of the updated flaw depth, a' , in the calculation of Γ_m .

Primary Membrane Stress With Zero Primary Bending Stress

The relation for the primary membrane stress at limit load, σ_m , with a primary bending stress of zero, is determined by setting σ_b in Eq. B-1 equal to zero and solving for σ_m . The resulting expression is

$$\begin{aligned}\sigma_m(a) &= \sigma_f [1 - (a/t) (\theta/\pi) - 2\psi/\pi] \\ \psi &= \text{Arcsin}[0.5(a/t)\sin\theta]\end{aligned}\tag{B-17}$$

The limit load bound is given by

$$SF \cdot S_{c-m} = \sigma_m(a)\tag{B-18}$$

where SF is the required safety factor on stress, and S_{c-m} is the allowable primary membrane stress with a primary bending stress of zero. $\sigma_m(a)$ is calculated by using the initial flaw depth, a , prior to any ductile flaw extension.

The failure assessment diagram coordinate S'_r is given by

$$S'_r = SF P_m / P'_m(a)\tag{B-19}$$

where $P'_m(a)$ is the primary membrane stress at reference limit load calculated from Eq. B-4 by using the flaw depth, a , updated with ductile flaw extension. By comparing Eqs. B-18 and B-19, the limit load cutoff, $S'_r{}^{\text{cutoff}}$, given by the limit load bound $P_m = S_{c-m}$, is written as

$$S'_r{}^{\text{cutoff}} = \sigma_m(a) / P'_m(a)\tag{B-20}$$

where the initial flaw depth, a , has been substituted in place of the updated flaw depth, a' , in the calculation of P'_m .

Comparison Between the Limit Load Cutoff and the Reference (5)
Analytical Limit Load Procedure for Combined Primary Stresses

In the current method the full safety factor, SF, is applied to both the primary membrane stress, P_m , and the primary bending stress, P_b . In the flaw evaluation procedures for ferritic piping in the Code Case N-463-1 (1), the allowable primary bending stress based on limit load is given by

$$S_c = [(\sigma_b(SF=1) + P_m)/SF] - P_m \quad (B-21)$$

Here the $\sigma_b(SF=1)$ is evaluated by using Eq. B-13 or B-14 with a safety factor, SF, on P_m of 1.0 where all evaluations are based on using the initial flaw depth, a , only.

The limit load procedure in (1) has the restriction that $P_b \geq P_m$, and $P_m \leq 0.5 S_m$ for normal operating and upset conditions, and $P_m \leq S_m$ for emergency and faulted conditions. The S_m is the design stress intensity. These restrictions do not apply to the FAD procedures.

The two procedures can be compared by evaluating the variation of the allowable combined stress ratio $(P_m+P_b)/\sigma_f$ with P_m/σ_f , where σ_f is the flow stress. Here P_b is set equal to the allowable primary bending stress, S_c . For the current procedure, the allowable stress ratio is given by

$$(P_m + P_b)/\sigma_f = [(\sigma_b(SF))/SF + P_m]/\sigma_f \quad (B-22)$$

where $\sigma_b(SF)$ is evaluated by using Eq. B-13 or B-14 with the full required safety factor on P_m . The method in (5) gives

$$(P_m + P_b)/\sigma_f = [(\sigma_b(SF=1) + P_m)/SF]/\sigma_f \quad (B-23)$$

The two procedures are first compared for an unflawed pipe. Eqs. B-22 and B-23 are compared for $a=0$ in Figure B-1 for SF=1.0 and SF=2.77. The two procedures produce the same results for flawed or unflawed pipe for SF=1.0. Figure B-2 is a reproduction of Figure B-1 with expanded scales to show further details. These figures are similar to the combined stress interaction diagrams used to define primary stress limits for pipe in ASME Section III NB3000 (8). The lines defining $P_b=P_m$ and $P_b=0$ are also plotted on Figures B-1 and B-2. The condition $P_b=0$ for the current procedure corresponds to the case where limit load has been reached on the

primary membrane stress alone. The region covered by the current procedure is bounded by the vertical axis, the line $P_b=0$ and the allowable $(P_m + P_b)/\sigma_f$ curve. The region covered by the procedure in (1) is bounded by the vertical axis, the line $P_b=P_m$, and the allowable $(P_m + P_b)/\sigma_f$ curve.

The current procedure and the procedure in (1) are in close agreement provided $P_b \geq P_m$, which is the range imposed by the restrictions in (1).

The ASME Section III design limits for normal operating conditions, of $P_m \leq S_m$ and $P_m + P_b \leq 1.5 S_m$, are also plotted on Figure B-2. The design boxes plotted are based on $\sigma_f = 2.4 S_m$ and $\sigma_f = 3.0 S_m$. In (1) a flow stress equal to $2.4 S_m$ was used. For $\sigma_f = 2.4 S_m$, both procedures enforce lower primary stresses than the ASME Section III design limits for the unflawed pipe. For $\sigma_f = 3.0 S_m$, the procedure from (1) is in good agreement with the design limit on $(P_m + P_b)/S_m$. The current procedure is in good agreement with the design limit for increasing values of P_m/σ_f out to the line $P_b=P_m$, beyond which the current procedure enforces lower primary stresses than the design limit.

The two procedures are compared for flaw sizes $a/t=0.20$, $\theta/\pi=0.20$ and $a/t=0.50$, $\theta/\pi=0.50$ in Figures B-3 and B-4. Comparisons were also made for several other flaw sizes. The trend was for the difference between the two procedures to increase with increasing flaw depth or increasing circumferential flaw length. The current procedure consistently enforced lower combined stresses as P_m approached or exceeded P_b .

The FAD approach given here also applies the full safety factor on P_m and P_b in the Elastic-Plastic Fracture Mechanics (EPFM) procedure. The application of safety factors for EPFM in (1) is treated the same as for the limit load procedure. Therefore, differences between the two procedures in the application of safety factors are also inherent for EPFM evaluations. Other differences between the two procedures also exist in the treatment of ductile fracture.

LIMIT LOAD CUTOFF FOR AXIAL FLAWS

An empirical formulation for the hoop stress at failure, σ_h , was developed previously in (9) for pipes with axial through-wall flaws and is

$$\sigma_h = \sigma_f/M_2 \quad (B-24)$$

where

$$M_2 = [1 + (1.61/4Rt)l^2]^{0.5}, \quad (B-25)$$

where l is the total flaw length, R is the mean radius of the pipe and t is the wall thickness of the pipe.

For part-through-the-wall axial flaws the hoop stress at failure is

$$\sigma_h(a) = \sigma_f \{ (1 - (a/t)) / (1 - (a/t)/M_2) \} \quad (B-26)$$

These equations are the same as used in (1,4,5). $\sigma_h(a)$ is calculated by using the initial flaw depth, a , prior to any ductile flaw extension. The limit load bound is given by

$$SF \cdot S_a = \sigma_h(a) \quad (B-27)$$

where S_a is the allowable hoop stress due to internal pressure, and SF is the required safety factor on stress.

The failure assessment diagram coordinate S'_r is given by

$$S'_r = SF \cdot p / p_0(a') \quad (B-28)$$

where p is internal pressure, and $p_0(a')$ is the internal pressure at reference limit load for a flaw depth, a' , updated with ductile flaw extension Δa .

$$p_0(a') = \sigma_y (2/\sqrt{3}) \{ t - a^* \} / [R_1 + a^*]$$

$$a^* = a' \{ 1 - 1/B_1 \} / [1 - (a'/t)/B_1]$$

$$B_1 = [1 + 0.5((a'/t)/(a'/l))^2]^{0.5}$$

$$a' = a + \Delta a \quad (B-29)$$

Here R_1 is the inner radius of the pipe. By multiplying both sides of Eq. B-27 by (t/R_1) , and comparing the result with Eq. B-28, the limit load cutoff, $S'_r{}^{cutoff}$, given by the limit load bound $pR_1/t = S_a$, is given by

$$s_{f}^{\text{cutoff}} = (t/R_1)\sigma_h(a)/p_0(a) \quad (\text{B-30})$$

The initial flaw depth, a , has been substituted in place of the updated flaw depth, \hat{a} , in the calculation of p_0 .

A second bound against plastic collapse is that the length of an axial part-through-the-wall flaw is limited by the through-wall flaw length at plastic collapse. This limiting flaw length, l_{crit} , is determined for a given hoop stress, given by pR_1/t , from Eqs. B-24 and B-25.

$$l_{\text{crit}} = 1.58(Rt)^{0.5} \{(\sigma_f/(pR_1/t))^2 - 1\}^{0.5} \quad (\text{B-31})$$

Here a safety factor of 1.0 on stress has been used. This is consistent with (1).

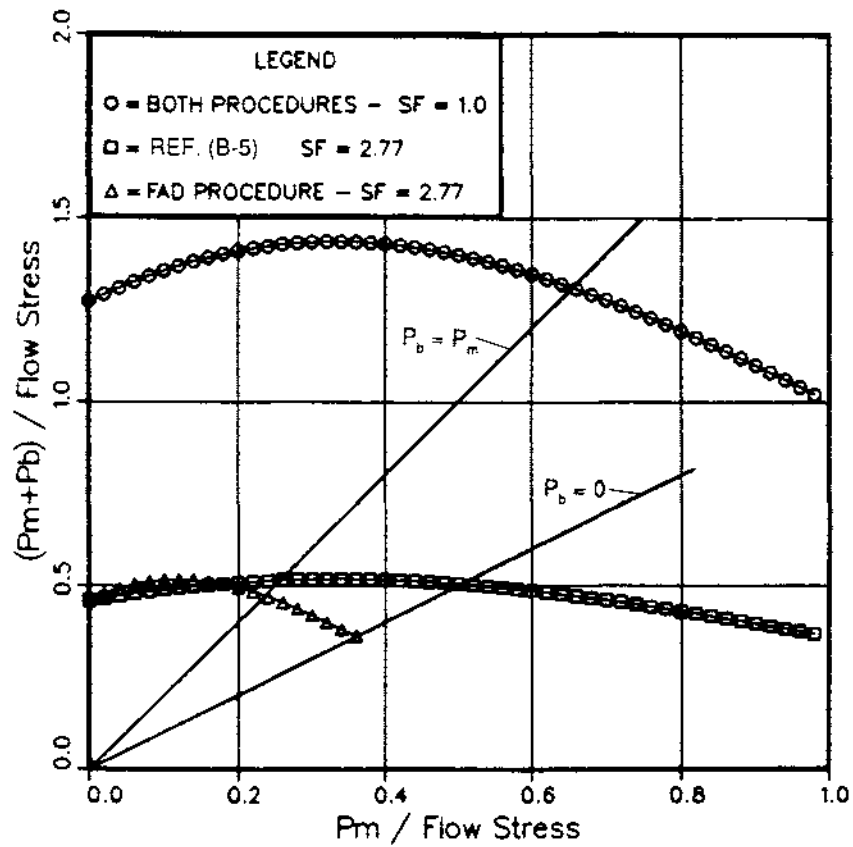


Figure B-1 Comparison of axial primary stress limits from the current FAD procedure and the procedure in (1) for an unflawed pipe using safety factors of 1.0 and 2.77.

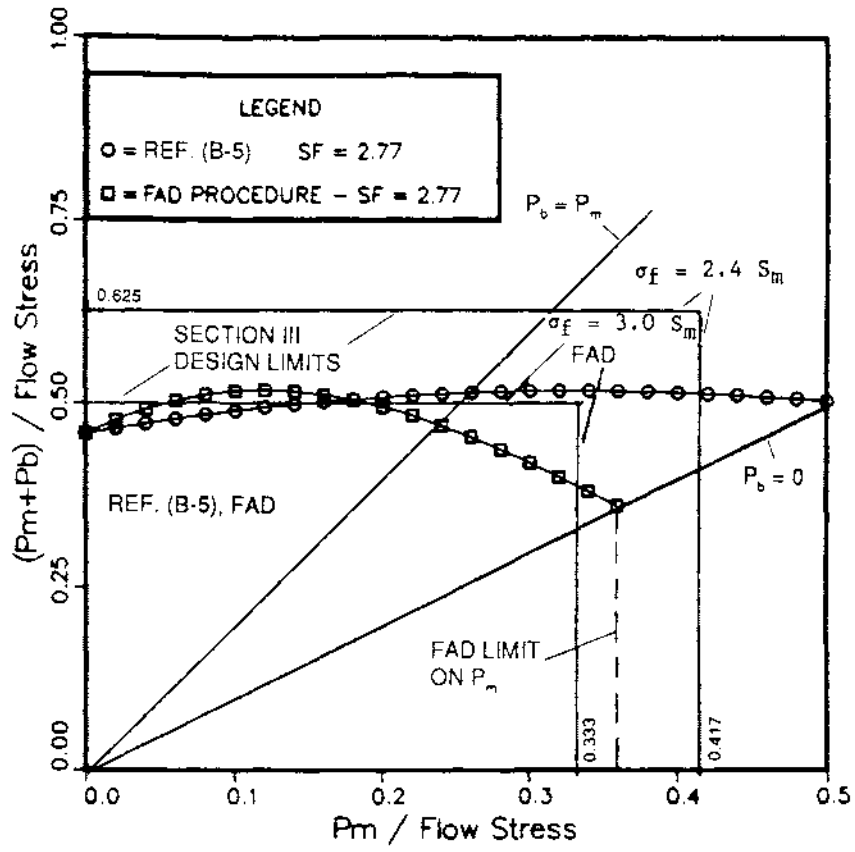


Figure B-2 Comparison of axial primary stress limits from the current FAD procedure and the procedure in (1) for an unflawed pipe using a safety factor of 2.77. Also shown are the ASME Section III design limits.

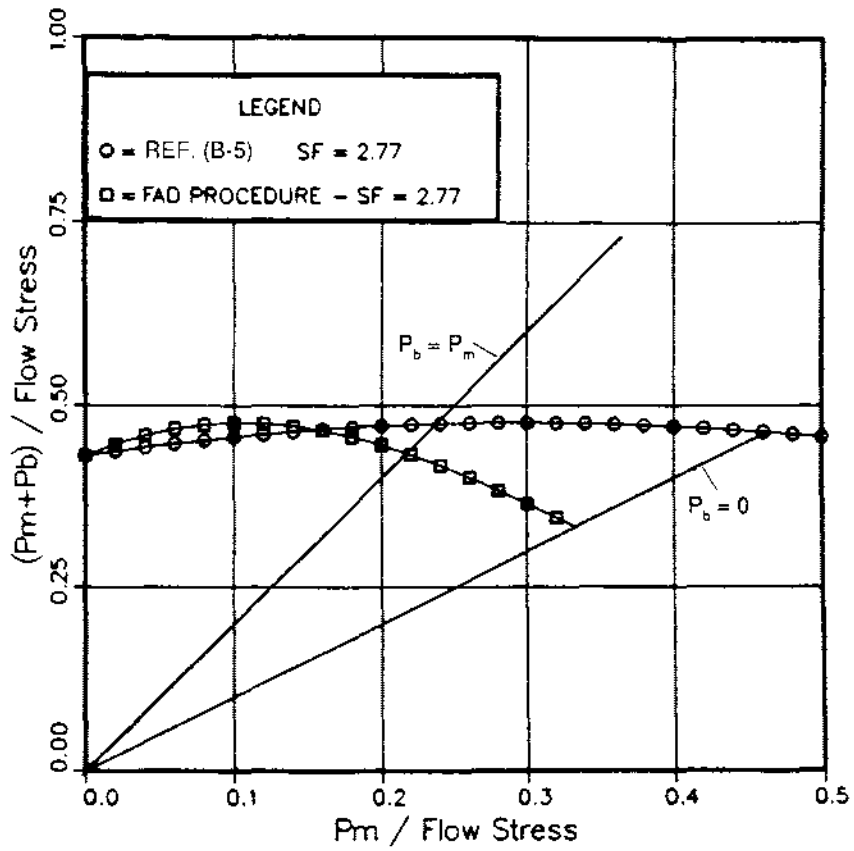


Figure B-3 Comparison of axial primary stress limits from the current FAD procedure and the procedure in (1) for a circumferentially flawed pipe with $a/t = 0.20$ and $\theta/\pi = 0.20$ using a safety factor of 2.77.

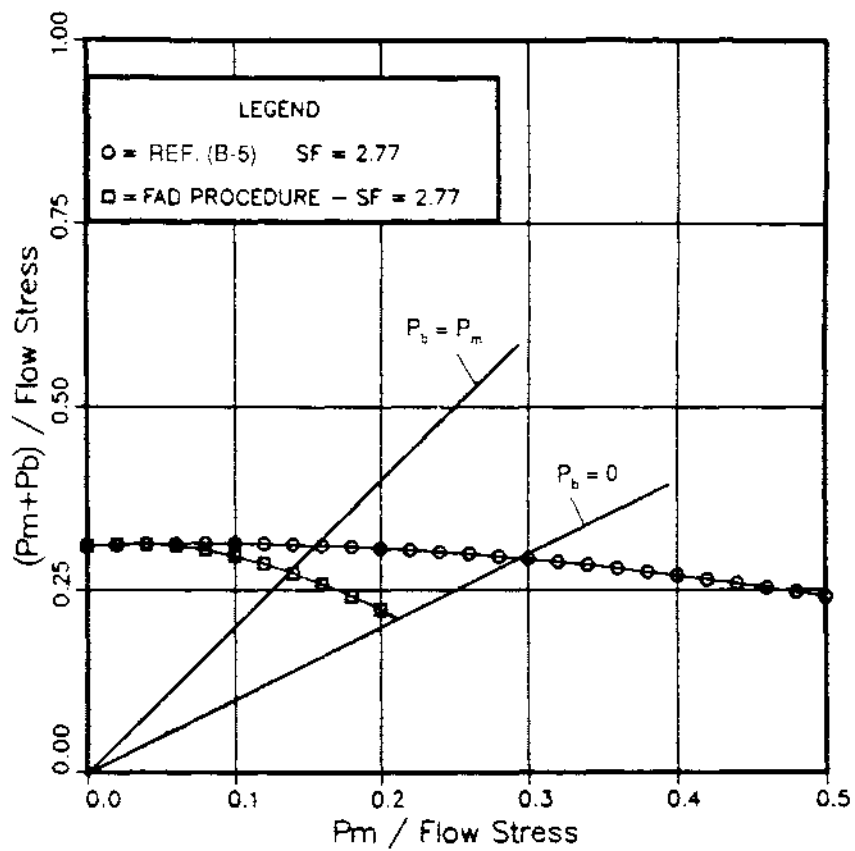


Figure B-4 Comparison of axial primary stress limits from the current FAD procedure and the procedure in (1) for a circumferentially flawed pipe with $a/t=0.50$ and $\theta/\pi=0.50$ using a safety factor of 2.77.

Appendix B

References

- B-1. "Evaluation Procedures and Acceptance Criteria for Flaws in Class 1 Ferritic Piping that Exceed the Acceptance Standards of IWB-3514-2, Section XI, Division 1", ASME Boiler and Pressure Vessel Code Case N-463-1.
- B-2. M.F. Kanninen, et al., "Toward an Elastic Plastic Fracture Mechanics Predictive Capability for Reactor Piping," Nuclear Engineering and Design, 48, 117-134, 1978.
- B-3. M.F. Kanninen, et al. "Instability Predictions for Circumferentially Cracked Type-304 Stainless Steel Pipe Under Dynamic Loading," Electric Power Research Institute Report NP-2347 (Vol. 1: Summary; Vol. 2: Appendices), April 1982.
- B-4. "Evaluation of Flaws in Austenitic Steel Piping," Prepared by the ASME Section XI Task Group for Piping Flaw Evaluation, ASME Boiler and Pressure Vessel Code Committee, EPRI Report NP 4690-SR, Electric Power Research Institute, Palo Alto, CA, April 1986; see also Journal of Pressure Vessel Technology, Vol. 108, 1986, pp. 352-366.
- B-5. "Evaluation of Flaws in Ferritic Piping", EPRI Report NP-6045, Research Project 1757-65, Electric Power Research Institute, Palo Alto, CA, October 1988.
- B-6. J.M. Bloom and S.N. Malik, "Procedure for the Assessment of the Integrity of Nuclear Pressure Vessels and Piping Containing Defects", EPRI Report NP-2431, Research Project 1237-2, Electric Power Research Institute, Palo Alto, CA., June 1982.
- B-7. J.M. Bloom, "Validation of a Deformation Plasticity Failure Assessment Diagram Approach to Flaw Evaluation," in Elastic Plastic Fracture: Second Symposium, Volume II - Fracture Resistance Curves and Engineering Applications, ASTM STP 803, C.F. Shih and J.P. Gudas, Eds., American Society for Testing and Materials, 1983, pp. II-206 to II-238.
- B-8. "Criteria of the ASME Boiler and Pressure Vessel Code for Design by Analysis in Section III", prepared by the ASME Section III Working Group on Plant Design, 1985.
- B-9. R.J. Eiber, et al., "Investigation of the Initiation and Extent of Ductile Pipe Rupture," Battelle Columbus Laboratories, Report BMI-1908, June 1971.

